Bull Volcanol (1992) 54:646-684

Bulletin of
Volcanology

The plinian eruptions of 1912 at Novarupta, Katmai National Park, Alaska

Judy Fierstein and Wes Hildreth

US Geological Survey, MS 910, 345 Middlefield Road, Menlo Park, CA 94025, USA

Received January 15, 1992/Accepted March 3, 1992

Abstract. The three-day eruption at Novarupta in 1912 consisted of three discrete episodes. Episode I began with plinian dispersal of rhyolitic fallout (Layer A) and contemporaneous emplacement of rhyolitic ignimbrites and associated proximal veneers. The plinian column was sustained throughout most of the interval of ash flow generation, in spite of progressive increases in the proportions of dacitic and andesitic ejecta at the expense of rhyolite. Accordingly, plinian Layer B, which fell in unbroken continuity with purely rhyolitic Layer A, is zoned from >99% to ~15% rhyolite and accumulated synchronously with emplacement of the correspondingly zoned ash flow sequence in Mageik Creek and the Valley of Ten Thousand Smokes (VTTS). Only the andesite-richest flow units that cap the flow sequence lack a widespread fallout equivalent, indicating that ignimbrite emplacement barely outlasted the plinian phase. On near-vent ridges, the passing ash flows left proximal ignimbrite veneers that share the compositional zonation of their valley-filling equivalents but exhibit evidence for turbulent deposition and recurrent scour. Episode II began after a break of a few hours and was dominated by plinian dispersal of dacitic Layers C and D, punctuated by minor proximal intraplinian flows and surges. After another break, dacitic Layers F and G resulted from a third plinian episode (III); intercalated with these proximally are thin intraplinian ignimbrites and several andesite-rich fall/flow layers. Both CD and FG were ejected from an inner vent <400 m wide (nested within that of Episode I), into which the rhyolitic lava dome (Novarupta) was still later extruded. Two finer-grained ash layers settled from composite regional dust clouds: Layer E, which accumulated during the D-F hiatus, includes a contribution from small contemporaneous ash flows; and Layer H settled after the main eruption was over. Both are distinct layers in and near the VTTS, but distally they merge with CD and FG, respectively; they are largely dacitic but include rhyolitic shards that erupted during Episode I and were kept aloft by atmospheric turbulence. Published models yield column heights of 23-26 km for A, 22-25 km for CD, and 17-23 km for FG; and peak mass eruption rates of $0.7\text{-}1\times10^8$, $0.6\text{-}2\times10^8$, and $0.2\text{-}0.4\times10^8$ kg s^{-1}, respectively. Fallout volumes, adjusted to reflect calculated redistribution of rhyolitic glass shards, are 8.8 km^3, 4.8 km^3, and 3.4 km^3 for Episodes I, II, and III. Microprobe analyses of glass show that as much as 0.4 km^3 of rhyolitic glass shards from eruptive Episode I fell with CDE and 1.1 km^3 with FGH. Most of the rhyolitic ash in the dacitic fallout layers fell far downwind (SE of the vent); near the rhyolite-dominated ignimbrite, however, nearly all of Layers E and H are dacitic, showing that the downwind rhyolitic ash is of 'co-plinian' rather than co-ignimbrite origin.

Introduction

In June 1912, some 60 h of eruptive activity in what is now Katmai National Park on the Alaska Peninsula produced 11 ± 4 km^3 of ash flow tuff (ignimbrite) and ~17 km^3 of fallout in one of the world's largest historic eruptions. From the vent at Novarupta, ash flows travelled as far as 23 km northwestward and filled what became known as the Valley of Ten Thousand Smokes (VTTS) (Griggs 1922; Hildreth 1983). In addition, at least four ash flows penetrated the nearby notch of Katmai Pass, crossed the chain of stratovolcanoes, and flowed another 10 km down the Pacific slope (Fig. 1). The flow deposits may be more than 100 m thick in the upper VTTS and are 10 m thick at eroded distal termini. Proximal high-energy flow veneers, commonly 1-3 m thick, but as thick as 13 m on Falling Mountain (Fig. 1), were deposited by (commonly turbulent) passing flows on all near-vent ridges. Three plinian sequences, two of which followed emplacement of the main VTTS ignimbrite, covered 120,000 km^2 with a cumulative ash layer >1 cm thick (Fig. 2). Coarse fallback ejecta and ignimbrite fill the vent to an unknown depth, and pumiceous fallout accumulated to >12 m thick as far as 4 km from vent. The sequence of fall units forms a gradually thinning composite wedge that is cumulatively 30 cm thick

Fig. 1. Location map of the Valley of Ten Thousand Smokes (*VTTS*) and vicinity, showing locations of measured fallout sections (*dots*). More distal sections are shown in Fig. 2. Valley-filling parts of the 1912 ash flow sheet are *stippled*; four flow units spilled south through Katmai Pass (*KP*). The Novarupta crater is shown by *heavy dashed lines* and the small Novarupta lava dome by the *inverted traingle*. Baked (*B*) and Broken (*X*) Mountains consist of Jurassic siltstones and sandstones of the Naknek Formation. Mount Cerberus (*C*) and Falling Mountain (*F*) are pre-1912 dacite domes, the latter truncated by the 1912 eruption. More than 15 additional andesite and dacite vents (*filled triangles*) occur within 3–10 km of Novarupta. Two vents (*open triangles*) destroyed in 1912 during caldera collapse are exposed near the north and south rims of Katmai caldera. Outlined lava flows from Southwest Trident erupted between 1953 and 1968 and overlie the 1912 ash flow sheet along Mageik Creek. Key sections numbered *1–7* here are illustrated in Fig. 3; many additional sections are located and illustrated in Figs. 12 and 15. Place-name abbreviations: Three Forks (*T*); Ukak Lobe (*U*); Overlook Hill (*O*); Windy Creek embayment (*Wc*); Whiskey Ridge (*W*); Lethe Hills margin of narrowest part of VTTS (*LH*); East and West Mageik Lakes (*ML*)

at Kodiak (170 km downwind) but only 20 cm thick at Brooks Camp, 50 km upwind of the vent (Fig. 2). Fall deposits are well-preserved except in areas of rugged snowclad terrain, and the ignimbrite is well-exposed except proximally where the sheet is only shallowly incised.

The Novarupta crater is a 2-km-wide, pumice-filled ovoid depression that truncates Falling Mountain (a pre-1912 dacite dome) and Baked and Broken Mountains, ridges of sandstone and shale of the Upper Jurassic Naknek Formation. Regional stratigraphic relations indicate that the Naknek extends to a depth of ~1500 m here and overlies ~3500 m of subhorizontal Mesozoic sedimentary and volcanic rocks that are neither exposed nearby nor represented in the suite of 1912 lithic ejecta; all 1912 sedimentary lithics are apparently of Naknek derivation. The lithic data thus imply that the vent was excavated to a depth no greater than 1500 m (Hildreth 1987). Arcuate fractures around the crater's perimeter are due in part to compaction and ductile deformation of welded fallback ejecta, and probably also in part to progressive backfilling of a complexly nested vent complex that underwent concentric step-faulting, slumping, and subsidence during the course of several eruptive episodes (Hildreth 1987).

Two-thirds of Mount Katmai's summit complex – 10 km east of Novarupta – collapsed in 1912, apparently owing to hydraulic transfer of magma beneath the nearby stratovolcanoes (Curtis 1968; Hildreth 1983, 1987, 1991). The Katmai caldera, areally larger than the Novarupta crater, so impressed the early investigators, Fenner and Griggs, that they thought Mount Katmai was the source of most of the 1912 fallout. Curtis (1968) demonstrated, however, that Novarupta was the only plinian vent active in 1912. In an extraordinary example of compensatory caldera collapse taking place elsewhere in the system, the structure of the Novarupta vent was preserved. Because there was no large-scale collapse at Novarupta, near-source deposits are preserved, vent dimensions can be estimated, and proximal field data can be used to constrain eruption modelling. Moreover, owing to the strong compositional zonation, we have been able to use rhyolite/dacite/andesite pumice-clast proportions to unravel stratigraphic complexities and to correlate proximal deposits with distal ones and ash flow deposits with contemporaneous fall deposits.

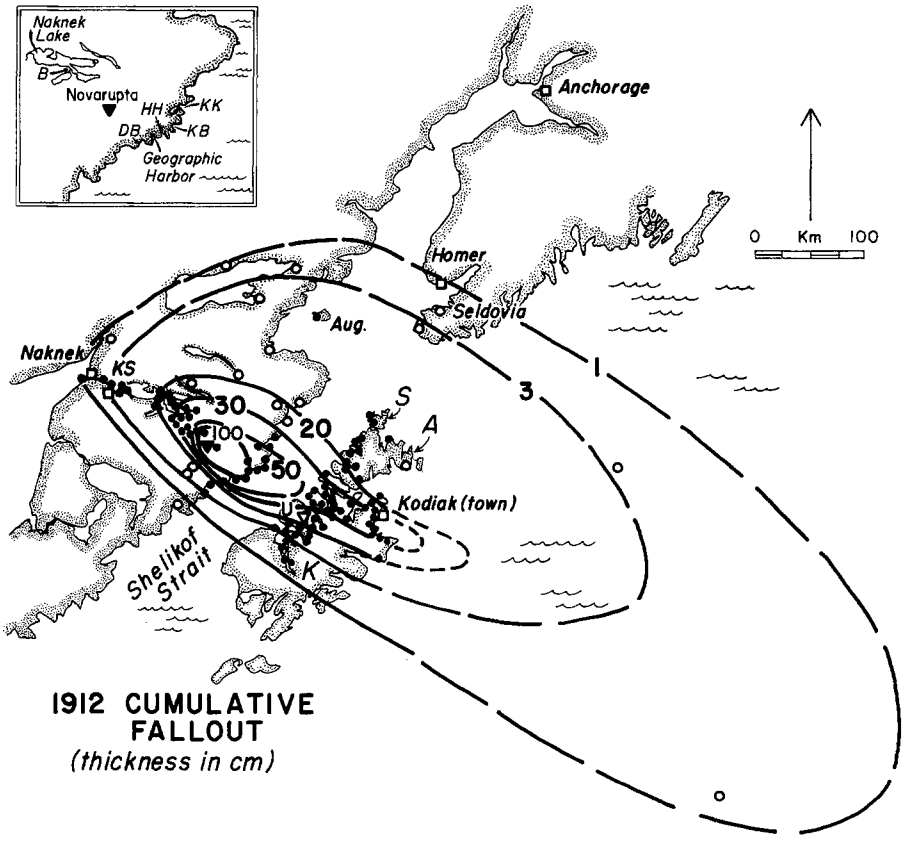

Fig. 2. Location map of the upper Alaska Peninsula showing the cumulative fallout from the three plinian eruptions that issued at Novarupta (*filled inverted triangle*) in 1912. *Filled circles* mark fallout sections measured in this study; open circles were reported by Martin (1913), Griggs (1922), Nayudu (1964), and JR Riehle (written communication 1983). *Open inverted triangle* is location of key section 9 in Fig. 3 at Uganik Bay (*U*) on Kodiak Island. *Open squares* are towns, as labelled. Other locations: *S* (Shuyak Island); *A* (Afognak Island); *K* (Kodiak Island); *Aug.* (Augustine Island); *B* (Brooks Camp); *KS* (King Salmon); *DB* (Dakavak Bay); *HH* (Hidden Harbor); *KB* (Kuliak Bay); *KK* (Kukak Bay)

Eruptive sequence

The 1912 eruption consisted of three main intervals of eruptive activity here called Episodes I, II, and III (Table 1). Each episode was complex, especially Episode I, which underwent a change in eruptive style from dominantly plinian (Layer A) – with subordinate associated pyroclastic flows – to dominantly valley-filling ash flows – with subordinate contemporaneous plinian fallout (Layer B). This change coincided with the introduction of dacitic and andesitic pumice clasts into a previously all-rhyolite eruption column. Episodes II and III were predominantly dacitic in composition and generated plinian fall layers CD and FG; each also included small intraplinian pyroclastic flows and surges.

Near-vent fallout deposits that were designated Layers A through I by Curtis (1968) in upper Knife Creek show more variability elsewhere, but his generalized stratigraphy can be applied with reasonable certainty, even as far downwind as Kodiak Island (Figs. 2 and 3). The basal deposit is rhyolitic fall Layer A, which underlies and intercalates with rhyolitic ignimbrite in the downwind direction (in Mageik Creek, Fig. 1) but is almost nowhere present in the VTTS. What Curtis called 'Layer B' in upper Knife Creek is a marginal facies of the VTTS ignimbrite; Layer B is herein redefined to include compositionally zoned fallout that overlies Layer A in the downwind sector (south and east of vent) and is time-correlative with most of the ash flow emplacement sequence in the VTTS (Fig. 4). There is no discontinuity between Layers A and B; they are compositionally distinct parts of a continuous fall deposit from a fluctuating but uninterrupted eruption column.

Emplacement of the rhyolitic-to-andesitic sequence of voluminous ignimbrites ($11 \pm 4\ km^3$) outlasted the plinian part of the first eruptive episode, but it was followed within hours by several dacitic plinian falls that overlie the ignimbrite in the VTTS and overlie Layer B in the downwind sector. Except for extremely distal tephra, the dacite layers are usually resolvable into two main sequences (Layers CD and FG of Curtis, the products of Episodes II and III, respectively). In and near the VTTS these are separated by a fine-grained, crystal-depleted, 5–9-cm-thick, vitric ashfall (Layer E) that accumulated during an extended break (probably a few hours) in plinian activity. Similar vitric ash (Layer H) that settled at the end of the explosive eruptive sequence caps the section. Locally developed, moderately well-sorted, crystal-rich sandy layers found atop or within Layer H in upper Knife Creek, are in part wind-reworked laminae but may include ashfalls from small explosions at Novarupta or from phreatic explosions at Mount Katmai and along Knife Creek (called 'Layer I' by Curtis 1968).

Sampling and methods

Grain-size parameters used to characterize the ejecta are based on Inman (1952), and the sieving process follows that described by Sparks (1976). Because the deposits are always damp, only particles 3.2 cm (-5ϕ) and larger

Table 1. Stratigraphic sequence of 1912 eruptive episodes at Novarupta

Eruptive unit (and associated subunits)	Composition (Rhy, Dac, And)	Maximum thickness (m)	Comments
Episode III			
Regional post-eruptive dustfall	D>R	0.3	• Forms separate layer (Layer H) proximally and medially; merges with F–G distally. Mostly dacitic in and near VTTS; up to 40% rhyolite to SE; up to ~20% rhyolite to NW
Plinian Layers F and G	D (<1% R, trace A)	> 10	• Regional fallout with relatively symmetrical dispersal; consists of 3 subunits (F_1, F_2, G), themselves locally internally stratified
intraplinian pyroclastic flows	D>A (+trace R)	< 3	• Limited to within 4 km of Novarupta; source of fine-grained partings in upper Knife Creek fallout within ~5 km of vent
Episode II			
Dustfall Layer E	D≫R>A	0.1	• Discrete layer only in and near VTTS; settled during plinian hiatus a few hours long
near-vent surges	D>A	1	• <3 km from vent (Fig. 12, sections 1 and 27)
interplinian pyroclastic flows	D>A	< 2	• <2.5 km from vent (Fig. 12, sections 19, 20 and 21)
Plinian Layers C and D	D (<1% R, trace A)	> 10	• Regional fallout with marked SE dispersal; consists of 3 subunits (C_1 C_2, D)
intraplinian pyroclastic flows	D (+minor A, R)	2	• <3 km from vent
near-vent surges	D≫R~A	2	• Exposed in patchy remnants on near-vent ridges
block-rich pyroclastic flows	D>A	< 2	• Restricted to proximal locations up to 4 km from vent; contemporaneous with basal part of Layer C
Episode I			
Main valley-filling ignimbrites (VFI)	R>D>A	>100	• Increasing dactic+andesitic components in later eruptive pulses; filled valleys both N and S of vent
marginal facies of ignimbrite	R (+minor D)	—	• Wedge of deposits along flow margins related to marginal turbulence or run-up
high-energy proximal ignimbrite (HEPI)	R+D>A	13	• Stratified proximal facies of valley-filling ignimbrite on near-vent ridgetops; increasing fraction of intermediate clasts upward. Like rhyolitic HEPI, deposited from upper zones of density stratified flows. Most exposures 1–4 m thick
Plinian Layer B			
Layer B_3	D>R (+minor A)	0.5	• Mostly S to ESE of source; only beyond VFI margins; contemporaneous with main VFI
Layer B_2			• Only S to ESE of source; none near vent or in VTTS; gradational transition from rhyolite to dacite as the major component; contemporaneous with main VFI
upper half	D>R (+minor A)	0.7	
lower half	R (+minor D, A)		
Layer B_1: composite of plinian lapilli + co-ignimbrite ash	R (+trace D, A)	0.1	• First appearance of dacite+andesite pumice; only in Mageik Creek drainage basin <13 km from vent; fine ash elutriated from a thin tongue of contemporaneous rhyolite-rich VFI mixed with fallout
All-rhyolite ignimbrites			
valley-filling ignimbrite (VFI)	R	13	• Massive flows exposed beyond the margins of the main overlying heterogeneous VFI in Katmai Pass, Mageik Creek, and Griggs Fork; VFI in Griggs Fork is direct run-up
marginal facies of ignimbrite	R	—	• Marginal facies of VFI can be vaguely stratified, wedging out 100s of m above valley floor
high-energy proximal ignimbrite (HEPI)	R	4	• Stratified and lenticular deposits on ridgetops as far as 9 km from vent; intercalated locally with rhyolite fallout; emplaced from concentrated but turbulent upper zones of density-stratified valley-filling flows
All-rhyolite plinian Layer A	R	1.4	• Regional fallout with ESE dispersal axis; none exposed or preserved near-vent except in Griggs Fork and Trident saddles; contemporaneous with rhyolitic pyroclastic flows

were sieved in the field; the remainder was dried, sieved, and weighed in the laboratory. The discrepancy thus introduced between dry and wet weights has not been corrected; because the very coarse fraction of collected samples is small, however, the error in weight percent is also small.

In order to promote consistency, 'channel' samples were taken through each layer in distal sections, and 'bottom' and 'top' samples were collected from the much thicker (usually graded) fall units in proximal sections. Bulk samples of ignimbrite were collected where no internal sorting was discerned, and 'coarse' and

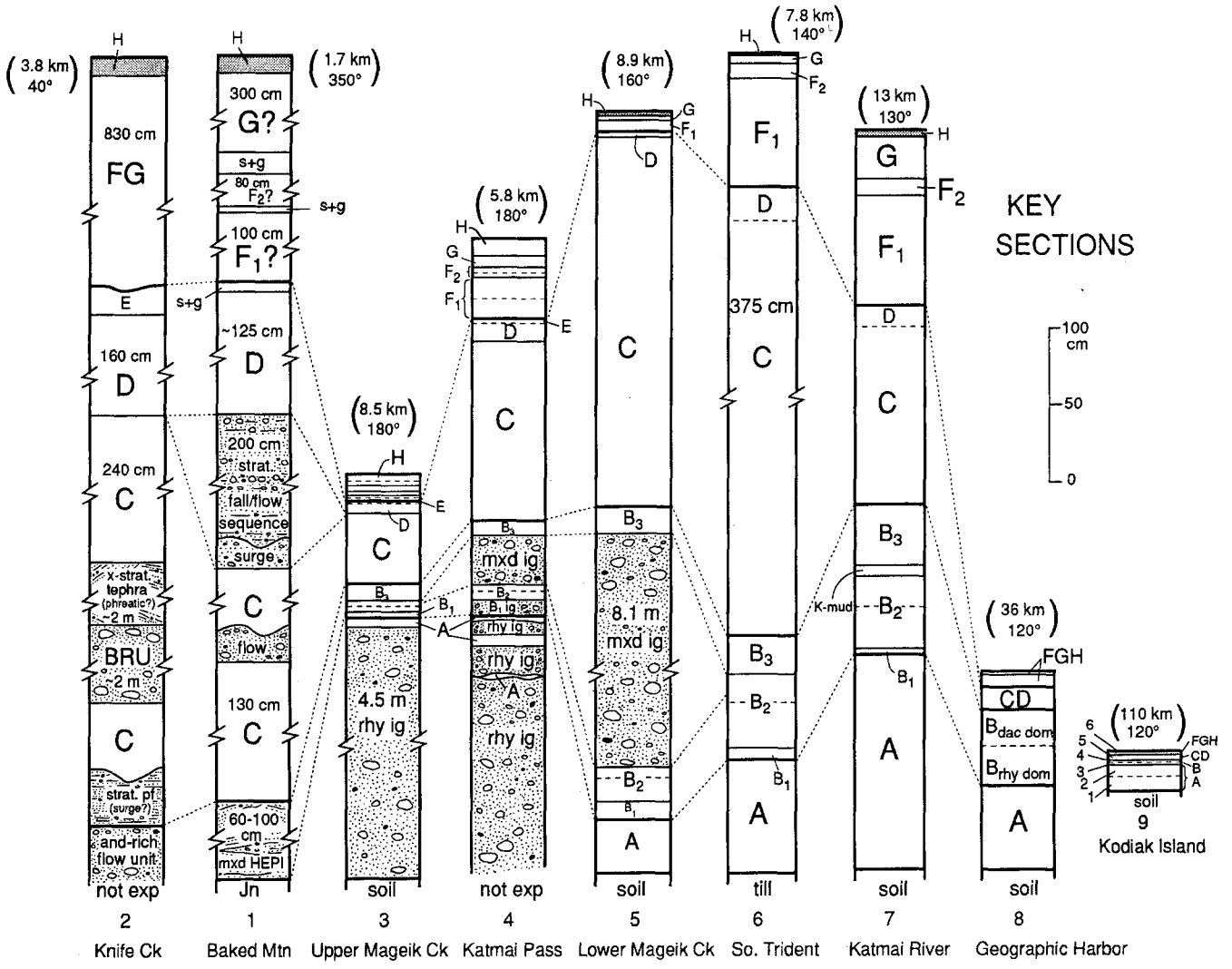

Fig. 3. Key sections referred to in text. Distance (in km) and azimuth from Novarupta are shown at the top of each section; locations are noted on Figs. 1 and 2. Deposit thicknesses are to scale (except where given, on broken columns); pumice (*open shapes*) and lithics (*filled shapes*) are not to scale. Basal rhyolitic plinian fallout (Layer A) and contemporaneous all-rhyolite ignimbrite were followed by the main zoned ignimbrite sequence (*mxd ig*), time-equivalent high-energy proximal ignimbrite (*mxd* HEPI), and associated fallout Layers B_1, B_2, and B_3, all compositionally heterogeneous. Andesite-rich (*and-rich*) flow unit in section 2 caps thick valley-filling ignimbrite of the VTTS. *Dashed lines* in B_2 represents abrupt increase in dacitic pumice clasts marking the transition between rhyolite-dominant (*rhy dom*) and dacite-dominant (*dac dom*) fallout. Plinian dacite falls of Episodes II and III (*Layers CD and FG*) are each capped by fine ash layers (*Layers E, H*). Composite intraplinian fall/flow sequence in section 1 has both fall and flow components. *BRU* is block-rich flow unit related to Layer C; *s+g* (section 1) refers to ultra-proximal intercalations of sandy crystal ash and pumice granules between coarse pumice falls. *K-mud* (section 7) refers to Katmai-derived phreatic ash related to caldera collapse. Color zones 1–6 (section 9) in distal ashfall are discussed in text

'fine' samples were collected where clast-size-delineated segregations occur. Maximum clast size is the averaged length of the three axes of the 3–5 largest pumice (MP) or lithic (ML) clasts within areas of 1-to-25 m^2 (depending on layer thickness).

Because stratigraphic details of the plinian deposits differ sectorially around the source and also change with distance from source, the plinian sequences that Curtis (1968) divided into Layers C, D, F and G in upper Knife Creek are not as simple south of Trident or in the central and lower VTTS; this has required subdivision of Layers C and F (see Figs. 3 and 12) in addition to redefinition of Layer B. The most reliable and regionally persistent correlation criteria are (1) the compositional distinction between initially rhyolitic, subsequently heterogeneous, and finally dominantly dacitic ejecta; and (2) stratigraphic position with respect to the distinctive Layers E and H. Measured sections are referred to throughout the text by the section numbers shown in Figs. 1, 2, 3, 12, and 15, and in Tables 2 and 3.

Eruptive Episode I (Phase A)

Initial plinian rhyolite: Layer A

The basal fall deposit in the downwind sector is plinian Layer A, which makes up ~15% of the total fallout on the southern slopes of Trident (6–8 km SE of vent),

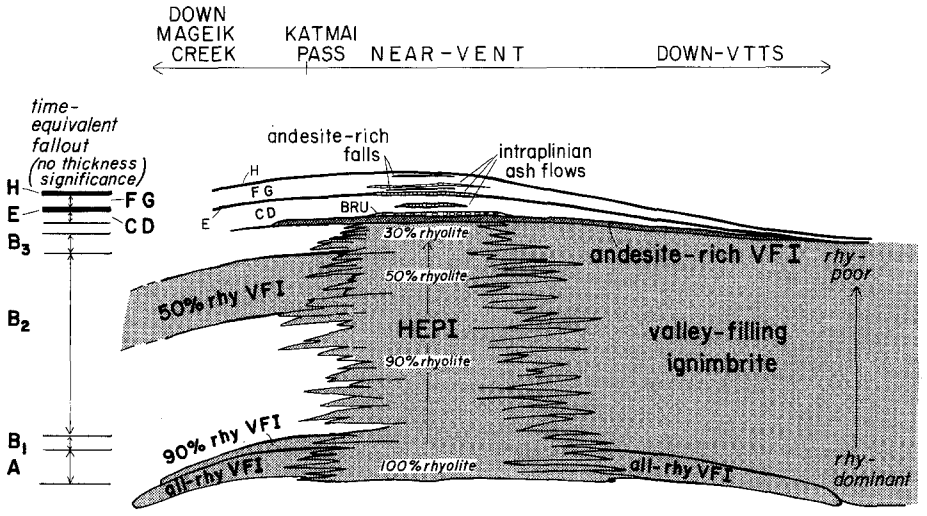

Fig. 4. Cartoon summarizing idealized 1912 stratigraphy (Table 1). 'Percent rhyolite' refers to both fall and contemporaneous flow deposits. All-rhyolite high-energy proximal ignimbrite (*HEPI*) and valley-filling flows (*VFI*) are contemporaneous with plinian Layer A. Sublayers of plinian Layer B are contemporaneous with heterogeneous VFI, which also has a high-energy proximal facies (*HEPI*) exposed near the vent; earliest HEPI deposits were partly scoured by later flows, so most HEPI deposits correlate with the upper VFI. Late andesite-rich flow units capping the main ignimbrite are less extensive than earlier rhyolite-rich flows; these late-stage flows had no contemporaneous regional fallout, indicating a brief hiatus in plinian activity between deposition of Layers B_3 and C. Intraplinian surges, ash flows and andesite-rich falls are intercalated proximally with plinian C–G; the most extensive of these are block-rich flow units (*BRU*) exposed in Novarupta Basin and intercalated in basal Layer C as far as 4 km NE

Table 2. Pumice clast proportions in 1912 deposits[a]

Location	Sample	Description	Rhyolite	Dacite	Andesite	Banded
High energy proximal ignimbrite (HEPI)						
Buttress Range						
Section 36	K-425	top	100	0	0	0
	K-424	middle	100	0	0	0
Section 52	K-747	base	100	0	0	0
Baked Mountain						
Section 1	K-565	top 10 cm	11	89	0	0
	K-374	middle	19	72	2	6
	K-563	basal 10 cm	14	73	12	2
Section 10	—	top	3	56	37	5
	—	middle	67	16	7	10
	—	base	100	0	0	0
Section 40	—	top	3	67	15	15
	—	middle	2	77	22	0
	—	bottom 1/3	3	68	11	18
Section 41	K-737	base	33	49	16	3
Section 12	K-584	top	18	78	2	2
	K-587	49 cm above base	14	84	1	1
	K-589	20 cm above base	29	54	13	4
	K-590	base	20	77	3	0
Section 11	K-594	25 cm below top	20	58	15	6
	K-593	basal 16 cm	29	62	8	1
Broken Mountain						
Section 42	K-844	top 10 cm	22	73	4	1
	K-843	basal 10 cm	20	79	1	0.5
Section 28	K-518	top	15	84	0	1
	K-525	300 cm from base	18	67	12	3
	K-527	270 cm from base	14	61	20	5
	K-536	93 cm from base	17	67	4	11

For continuation of table please see the next page

Table 2. (continued)

Location	Sample	Description	Rhyolite	Dacite	Andesite	Banded
Falling Mountain (W edge of scarp)						
Section 22	K-569	top	22	75	0	4
	K-568	50–70 cm from base	17	44	35	4
	K-567	40–60 cm from base	22	48	30	0
	K-566	base	11	75	14	1
Whiskey Ridge						
Section 30	K-850	top	26	71	1	1
	K-849	~360 cm from base	100	0	0	0
	K-848	170 cm from base	100	0	0	0
	K-847	165 cm form base	100	0	0	0
	K-846	base	100	0	0	0
Trident Volcano						
Section 45	K-369	base	96	2	0	2
Valley-filling ignimbrite (VFI)						
River Lethe (W-central VTTS)						
Section 91	—	late flow unit top	27	21	45	7
Moraine Creek (central VTTS)						
	—	mxd ignimbrite top	66	2	32	0
	—	mxd ig 4 m from top	64	3	33	0
	—	mxd ig, exposed base	89	0.5	10	0
Knife Creek (upper VTTS)						
Section 109	—	mxd ignimbrite top	6	59	35	0
	—	mxd ignimbrite top	13	52	35	0
Section 111	K-402	mxd ignimbrite	61	34	3.5	1
Trident (lower S flank)						
Section 92	—	B_1-ignimbrite top	88	10	0	2
	—	B_1-ignimbrite base	95	0	0	5
Mageik, Creek						
Section 5	—	mxd ignimbrite top	51	47	1	1
	—	mxd ignimbrite base	52	47	1	0
Section 93	—	mxd ignimbrite top	54	36	8	2
	—	mxd ignimbrite base	29	65	6	0
Section 95	—	mxd ignimbrite top	37	56	11	0
Section 53	K-818	all-rhy ignimbrite top	100	0	0	0
Section 94	—	all-rhy ignimbrite	100	0	0	0
Katmai Pass						
Section 4	—	mxd ignimbrite	42	45	6	7
	—	all-rhy ignimbrite	100	0	0	0
Section 54	K-256	all-rhy ignimbrite	100	tr.	0	0
Griggs Fork (direct run-up)						
Section 29	K-627	all-rhy ig. basal 1-m	100	0	0	0
Section 43	K-628	all-rhy ignimbrite base	100	0	0	0
Marginal facies of VFI						
Mount Griggs (W foot)						
Section 46	K-400	top	97	3	0	0
	K-401	base	99	1	0	0
Section 107	K-238	top	99	0.6	0	0.3
Section 47	K-234	top	100	0	0	0
	K-233	base	100	0	0	0
Section 44	K-740	base, Juhle Fork	99	0.4	0.2	0.2
Mount Mageik (SE flank)						
Section 49	K-817	basal 10 cm	100	0	0	0
Section 50	—	base	75	22	3	0
Mount Mageik (N flank)						
Section 51	K-621	top	68	14	11	7
	K-620	middle	42	53	2	2

For continuation of table see the next page

Table 2. (continued)

Location	Sample	Description	Rhyolite	Dacite	Andesite	Banded
Fallout						
Trident Volcano (S flank)						
Section 55	—	B_3	37	60	3	0
	K-837	B_2, top	36	61	2	1
	K-836	B_2, base	93	4	3	1
	K-835	A, base	100	0	0	0
Mount Griggs (Juhle Fork)						
Section 44	K-739	B_3	31	65	1	2
Mount Grigs (Griggs Fork)						
Section 98	—	B_2, middle	64	33	0	2
Section 99	—	C, base	9	86	1	4
	—	B_3?	12	86	0	2
Mount Griggs (W flank)						
Section 102	K-397	FG	3	97	0.3	0.5
	K-398	D(?)	4	94	1	1
Upper Knife Creek						
Section 103	K-379	F, base	0.3	99	0.3	0.1
	K-383	C, base	14	85	1	0
Section 105	—	G	0	>99	0	<1
	—	F	<1	>99	0	0
	—	C	<1	>99	0	0
River Lethe						
Section 104	K-347	F, base	0.5	99	0	0
	K-353	C, base	9	90	0.7	0.3
Mageik Creek						
Section 5	K-823	B_2, middle	73	19	4	3
	—	B_2, base	91	8	1	0
	K-822	A, base	100	0	0	0
Section 53	—	eroded top of C	6	93	1	0
	—	B_3	21	69	10	0
Section 39	K-830	F	9	90	0	0.3
	K-829	D	4	88	0	8
	K-828	B_3(?)	23	76	0.2	0
	K-827	B_2, top	57	36	5	3
	K-826	B_2, base	88	5	4	2
	K-825a	B_1, lapilli	89	5	4	1
	K-825a	B_1, fine ash	99	1	0	—
	K-825	A, 40 cm from base	100	0	tr.	0
	K-824	A, base	100	0	0	0
Section 94	—	C, base	10	89	0.4	0.9
	—	B_3, top	19	75	6	0
Section 95	—	B_2	69	27	4	0
	—	A	100	0	0	0
Section 96	—	C	0	100	0	0
	—	B_1, lapilli	94	3	0	3
Section 97	—	B_2, top	43	43	7	9
	—	B_2, base	89	3	3	5
	—	B_1, lapilli	96	2	2	0
Katmai Pass						
Section 18	K-580	F	1	99	0	0
	K-579	D	0	100	0	0
	K-578	C	6	94	0	0
Section 4	—	F, base	5	94	0	1
	—	C, top	1	99	0	0
	—	C, base	10	89	1	0
	—	B_3	15	81	4	4
	—	B_2, top	40	41	10	9
	—	B_2, base	51	27	11	11
	—	B_1, lapilli	88	12	0	0
	—	A	100	0	0	0

For continuation of table see the next page

Table 2. (continued)

Location	Sample	Description	Rhyolite	Dacite	Andesite	Banded
Falling Mountain						
Section 22	K-571	C, middle	8	91	1	0
	K-570	C, base	6	94	0	0
Mount Cerberus						
Section 100	—	B_3(?) atop HEPI	19	78	3	0
Butress Range						
Section 56	K-754	FG	tr.	99	1	0
	K-756	D	15	85	0	0
	K-758	C_1	20	79	1	0
Broken Mountain						
Section 42	K-842	B_3	27	73	0.4	0.2
Mount Katmai (S flank)						
Section 74	K-1032	B_2 top	46	34	17	3
	K-1031	A, middle	100	0	0	0
	K-1030	A, near base	100	0	0	0
Section 75	K-1049	B_2 eroded top	83	3	4	10
	K-1048	B_2 base	73	2	0.2	24
	K-1047	B_1, lapilli	82	11	0	7
	K-1047	B_1, fine ash	99	0	0	—
	K-1046	A, top	99.7	0	0	0.2
	K-1043	A, base	100	0	0	0
Section 77	K-1118	B_3	15	83	0.1	2
	K-1117	B_2 top	17	59	3	20
	K-1116	B_2 base	86	4	0	9
	K-1115	B_1, lapilli	99	0.7	0	0.3
	K-1115	B_1, fine ash	100	0	0	—
Katmai River						
Section 7	K-1017	G, base	12	87	1	0
	K-1016	F_2	6	94	0	0
	K-1013	F_1, top	12	88	0	0
	K-1012	F_1, base	12	84	0	4
	K-1011	D	9	91	0	0
	K-1010	C, base	5	91	4	0
	K-1008	B_3 middle	11	87	2	0
	K-1005	B_2 top	20	42	35	2
	K-1004	B_2 middle	85	1	0	14
	K-1003	B_2 base	87	5	3	5
	K-1002	B_1, lapilli	99	0	0	1
	K-1002	B_1, fine ash	100	0	0	—
	K-1001	A, base	93	1	0	5
	K-1000	A, base	100	0	0	0
Section 76	K-1087	G	12	82	0.6	0.7
	K-1085	F_2(?)	16	74	0	0
	K-1083	F_1	7	90	1	1
	K-1080	C, base	6	94	0	tr.
	K-1077	B_3 top	11	87	0	2
	K-1074	B_3 base	21	76	1	2
	K-1073	B_2	72	17	0.3	11
	K-1068	B_2 base	89	2	0.1	8
	K-1067	B_1, lapilli	87	6	1	6
	K-1067	B_1, fine ash	99	1	0	—
	K-1079	A, top	100	0	0	0
	K-1065	A, middle	100	0	0	0
	K-1062	A, base	100	0	0	0
Geographic Harbor						
Section 8	K-914	FG	7	93	0	0
	K-915	CD	11	89	0	0
	K-916	B_{2-3} top	25	75	0	0.1
	K-917	B_{2-3} middle	38	59	0	3
	K-918	B_2 base	91	2	0.5	6
	K-919	A, top	98	0	0	2
	K-920	A, base	100	0	0	0

For continuation of table see the next page

Table 2. (continued)

Location	Sample	Description	Rhyolite	Dacite	Andesite	Banded
Inter- and Intraplinian units						
Baked Mountain						
Section 1	K-509	'surge' within CD	3	87	6	4
	K-506	'surge' within CD	7	84	7	2
Falling Mountain						
Section 19	K-582	pf between CD & FG time-equivalent to E	30	61	4	6
Novarupta (eiecta ring)						
Section 26	K-616	pf within FG	0	91	9	0
Trident (W)						
	—	BRU within basal C	tr.	85	14	1.5

[a] Clast proportions for coarse deposits determined in the field and/or lab by point-counting R/D/A/B pumice clasts of approximately similar size (modal %); Proportions for more distal and finer-grained deposits on the S flank of Mount Katmai and at Geographic Harbor determined by weighing R/D/A/B clasts from a range of sizes to as fine as 1 mm (wt%). Layer B_1 'lapilli' proportions determined by point-counting pumice clasts; B_1 'fine ash' proportions are based on shard point counts using the electron microprobe (see Table 3b for representative shard compositions). Numbered sections (Section x) are located in Figs. 1, 2, 12 and 15

Table 3a. Glass shard proportions in fine-grained ashfalls[a]

Location, km from vent	Bearing[b]	Fallout section	Total thickness (cm)	Sample	Color zone[c]	Rhyolite	Dacite	Andesite
Kodiak Island								
NW coast,								
97 km	135	57	2	K-679	6	39	61	0
				K-678	1	100	0	0
NW coast,								
113 km	125	58	12–13.5	K-672	6	25	75	0
				K-673	2	100	0	0
				K-674	1	100	0	0
NW coast (Uganik Bay),								
111 km	120	9	24	K-688	6	29	71	0
				K-689	5	37	63	0
				K-690	4	77	23	0
				K-691	3	90	10	0
				K-692	2	100	0	0
				K-693	1	100	0	0
N coast,								
119 km	107	59	21–25	K-660	6	29	71	0
				K-661	5	50	50	0
				K-662	3	63	37	0
				K-663	1	100	0	0
Afognak Island								
NW coast,	90	60	10.5	K-707	6	40	59	0
132 km				K-708	4, 5	24	76	0
				K-709	1	100	0	0
Shuyak Island,								
155 km	80	61	6.5	K-711	6	23	77	0
				K-710	3, 4	71	29	0
Augustine Island								
160 km	36	66	4	Aug-4		10	88	1
Geographic Harbor								
36 km	120	8	9.5	K-913	FGH, middle	41	55	3
Hidden Harbor								
40 km	113	82	26	K-889	FGH, top	39	53	8
Kuliak Bay								
55 km	99	83	74.5	K-880	Top	29	64	7
Kukak Bay								
57km	85	81	74	K-871	Top	29	61	8

For continuation of table see the next page

Table 3a. (continued)

Location, km from vent	Bearing[b]	Fallout section	Total thickness (cm)	Sample	Color zone[c]	Rhyolite	Dacite	Andesite
W of Overlook Hill								
20 km	305	64	16.5	K-472	Base	3	97	0
Naknek Lake								
32 km	330	65	28–29	K-854	Top	7	92	1
				K-853	Base	15	84	0
Brooks Camp,								
49 km	310	63	20	K-473	Top	19	79	1
				K-474	Base	9	87	4
King Salmon,								
100 km	299	62	2	K-862		1	98	1
VTTS and Vicinity								
Layer E								
Mt. Griggs, Juhle Fk, 9 km	345	70	8	K-742		7	89	5
Windy Creek, 14 km	320	69	7	K-790		3	92	5
Ukak lobe, VTTS, 15 km	320	33	9	K-285		11	86	3
SW corner, VTTS, 7 km	260	68	3.5	K-416		4	95	1
Layer H								
Baked Mtn., 3 km	320	11	12	K-732		0	100	0
Mt. Griggs, Juhle Fk, 9 km	345	70	12	K-741		1	99	0
Windy Creek, 18 km	325	106	4	K-803		13	87	0
VTTS Narrows, 12 km	315	84	4	K-464		0	100	0
Overlook Hill, 13 km	310	71	4	K-391		33	57	10
Buttress Range, 7 km	290	72	8	K-748		5	90	5
W. Mageik Lake, 7 km	270	80	10	K-361		0	100	0
E. Mageik Lake, 6 km	240	79	12	K-354		13	84	3
So. Katmai Pass, 6 km	180	37	6	K-436		0	100	0
Katmai River, 13 km	130	76	5	K-1089		2	98	0
E of Novarupta, 3 km	80	78	27	K-448		0	98	2

[a] Rhyolite/dacite/andesite shard proportions were determined by analyzing 65–170 shards per sample, effectively employing the Menlo Park ARL SEMQ 9-channel microprobe (15 Kv; 10 na; 10-s counts) as a point-counting device. Shard types are readily distinguished by their Ca, Mg, Fe and Ti contents (Table 3b)

[b] Bearing is from center of Novarupta lava dome

[c] Color zones (1–6) are as explained in text. 'Top' and 'Base' of fallout were commonly sampled when no internal structure was apparent

Table 3b. Representative microprobe analyses of glass shards from 1912 fallout and of Novarupta dome

	Rhyolite	Rhyolite	Dacite	Andesite	Rhyolite lava dome
	Kodiak I. (6)	*K-854* (3)	*K-854* (8)	*K-854* (3)	*K-16* (9)
SiO_2	78.49 (0.57)	78.83 (0.55)	76.63 (0.78)	72.87 (0.15)	78.07 (0.41)
TiO_2	0.14 (0.03)	0.19 (0.04)	0.34 (0.06)	0.58 (0.005)	0.17 (0.04)
Al_2O_3	12.22 (0.35)	12.15 (0.33)	12.84 (1.16)	14.50 (0.25)	12.54 (0.34)
FeO	1.10 (0.05)	1.25 (0.05)	1.68 (0.10)	2.52 (0.11)	1.12 (0.31)
MnO	0.07 (0.01)	0.06 (0.02)	0.05 (0.02)	0.07 (0.04)	0.04 (0.02)
MgO	0.09 (0.02)	0.14 (0.02)	0.26 (0.03)	0.58 (0.05)	0.10 (0.02)
CaO	0.77 (0.02)	0.89 (0.01)	1.29 (0.09)	2.63 (0.21)	0.69 (0.03)
Na_2O	4.21 (0.08)	3.41 (0.35)	3.98 (0.16)	3.72 (0.42)	3.90 (0.16)
K_2O	2.91 (0.13)	3.10 (0.02)	2.93 (0.09)	2.55 (0.06)	3.38 (0.06)
Total	100.00	100.00	100.00	100.01	100.01

- Data are averages of several microprobe analyses (no. in parenthesis) for which original totals were >98 wt% (except for K-16 with totals >96 wt%), here recalculated to 100 wt%. Standard deviations (in parentheses) follow each analysis. Glass shards are all rhyolitic, but glass derived from phenocryst-rich bulk pumice of dacitic (63–65% SiO_2) and andesitic (57–61% SiO_2) compositions are easily distinguished by microprobe, principally by their Ca, Mg, Fe, and Ti contents
- Kodiak Island (Uganik Bay) analyses include two each from samples K-691, K-692, and K-693, which are from color zones 1, 2, and 3, respectively (see Table 3a); sample K-16 is the Novarupta lava dome; sample K-854 is fallout at the N base of Mount Katolinat

Table 4. Representative component analyses of 1912 deposits[a]

Location	Fallout subunit[b]	Sample	Km from dome	Crystal wt%	Lithic wt%	Vitric[c] wt%
Layer A						
So. flank Trident		K-835 (base)	7.2	3	24	73
Katmai River		K-1064 (base)	13	2	23	75
Dakavak Bay		ARJ-90F (base)	40	4	11	85
Kukak Bay		ARJ-98D	42	9	9	82
Kodiak airport		K-268 (top)	170	12	1	87
		K-267 (middle)	170	3	0	97
		K-266 (base)	170	10	1	89
Layer B						
So. flank Trident	B_3	K-1200 (middle)	7.7	27	0.5	73
	B_2	K-836 (base)	7.7	6	17	76
Mageik Creek (base)	B_3	K-434	8.5	24	4	72
Katmai River	B_3	K-1008 (middle)	13	24	tr	75
	B_2	K-1003	13	4	6	91
Dakavak Bay	B_2	ARJ-90D (top)	40	14	6	80
Layer CD						
Upper Knife Creek	C_1	K-457	3.8	42	7	51
	C_1	K-403	5.1	36	3	61
	D	K-404	5.1	44	2	54
Mount Griggs (foot)	C	K-399	6.3	37	3	60
	D?	K-398	6.3	43	4	53
Buttress Range	C_1	K-423	8.1	60	2	38
NW VTTS (Ukak lobe)	C_1	K-286	19	67	tr	33
Dakavak Bay	C	ARJ-90C	40	45	tr	55
	C	ARJ-90B	40	49	0	51
Kodiak Island	CD	K-689	110	22	0	78
Layer FG						
Upper Knife Creek	F_1	K-455	3.8	55	1	44
Mount Griggs (foot)	F?	K-397	6.3	40	5	55
Mageik Creek	F_1	K-431	8.5	36	5	59
	G	K-433	8.5	62	1	37
Dakavak Bay	FG	ARJ-90A	40	56	1	43
Kukak Bay	FG	ARJ-98B	42	48	tr	52
Layer E						
Upper Knife Creek		K-456	3.8	13	1	87
Upper River Lethe		K-348	8.8	19	tr	81
Buttress Range		K-755	8.8	10	tr	90
Windy Creek		K-790	14	7	tr	93
		K-805	17	4	tr	96
NW VTTS (Ukak lobe)		K-285	19	9	tr	91
Layer H						
Baked Mountain		K-732	2.3	12	0.4	87
Upper River Lethe		K-1354	8.8	5	0.05	95
Windy Creek		K-803	17	12	0.1	88
High-energy proximal ignimbrite (all rhyolite)						
Baked Mountain (summit)		K-1254	2.4	1	12	87
Whiskey Ridge		K-849	5.3	0.6	9	90
Buttress Range		K-425 (top)	8.1	17	10	73
		K-424 (middle)	8.1	20	14	66
Marginal flow facies (all rhyolite)						
Mount Griggs (foot)		K-234	5.6	6	5	88
		K-233 (base)	5.6	3	6	91
Main valley-filling ignimbrite (mixed composition)						
Lower VTTS (Moraine Creek)		K-333 (fine)	14.4	2	6	92
(base of flow)		K-334 (coarse)	14.4	2	4	94
Lower VTTS (Ukak lobe)		K-287 (fine)	20.1	3	2	95
(middle of flow)		K-288 (coarse)	20.1	7	3	91
Central VTTS, eastern margin (Juhle Fork)		K-384 (bulk)	9.7	4	1	94
Upper VTTS (near Mount Cerberus) (top of main, rhy-rich flow)		K-444 (bulk)	4.8	31	2	67
Upper VTTS (Griggs Fork) (dark-matrix, late flow unit)		K-402 (bulk)	6.0	21	4	75

For continuation of table see the next page

Table 4. (continued)

Location	Fallout subunit[b]	Sample	Km from dome	Crystal wt%	Lithic wt%	Vitric[c] wt%
High-energy proximal ignimbrite (mixed composition)						
Trident Volcano (N)		K-369	2.8	9	8	83
Baked Mountain (SE spur)		K-374	1.5	38	3	59
Baked Mountain (summit)		K-1260 (coarsest zone)	2.4	23	0.8	77
		K-1259 (base)	2.4	21	6	73
Falling Mountain		K-569 (top)	1.2	51	0.6	48
		K-406 (middle)	1.2	47	16	37
Marginal flow facies (mixed composition)						
Buttress Range		K-227	11.1	2	tr	98
		K-229 (base)	11.1	11	tr	89
Mount Griggs		K-236	6.2	11	1	88

[a] Component analyses by point-counting size fractions >1 mm and heavy liquid separations of finer fractions; volume % converted to wt% using densities of 2.67, 2.6, and 1.0 for crystals, lithics, and pumice, respectively

[b] Fallout subunits are designated as in text. Subunit distinction fades with distance from source; thus, CD and FG are the total undifferentiated fallout layers for Episodes II and III, respectively

[c] 'Vitric' fraction includes pumice clasts. 'Crystals' are free grains. 'Lithics' are mostly Naknek Fm. Sedimentary rocks or vitrophyre containing fragments of Naknek

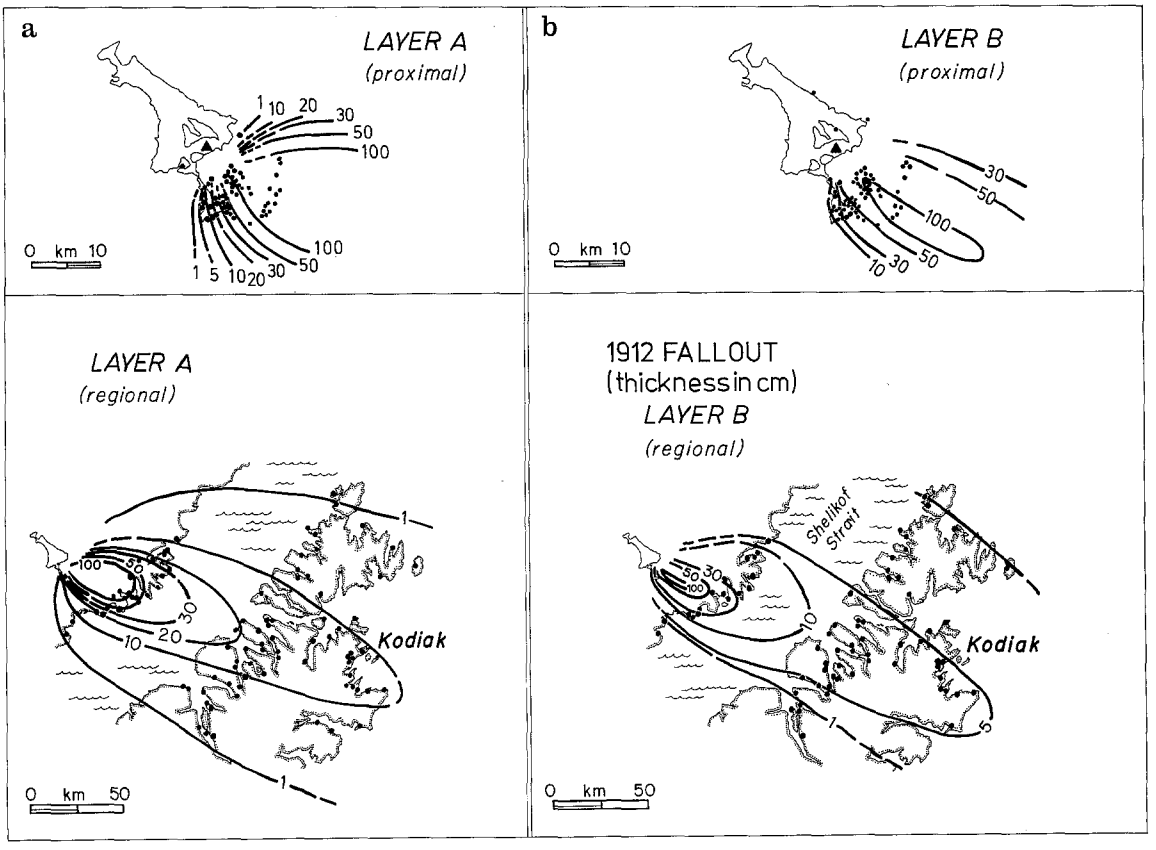

Fig. 5. a Isopachs of rhyolitic initial plinian Layer A (Phase A of Episode I). Fallout is strongly directed SE, mostly within a 90° sector from the vent. The thickness maximum is displaced SE of vent due to wind and contemporaneous high-energy flows that scoured near-vent fallout; a few centimeters of Layer A are intercalated with all-rhyolite (HEPI) flows 7 km NE and 5 km SE of source but is otherwise not found near and upwind of vent. **b** Isopachs of compositionally heterogeneous, plinian Layer B (Phase B of Episode I). Although there was no interruption in plinian deposition, Layer B is plotted separately from Layer A, because its base marks the incoming of dacitic and andesitic pumice clasts; it was contemporaneous with the main, compositionally heterogeneous ignimbrite in the VTTS. *Filled triangle* marks Novarupta; *dots* indicate measured sections. Outline of VTTS as in Fig. 1; shorelines as in Fig. 2

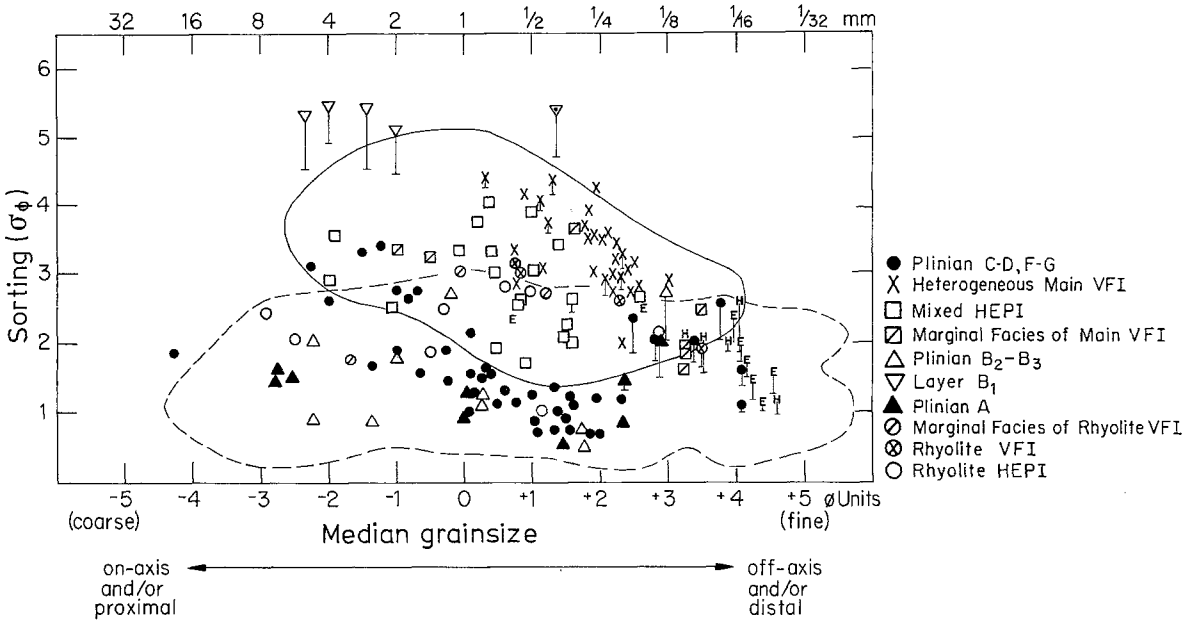

Fig. 6. Median grain size (Md_ϕ and mm) and sorting coefficient (σ_ϕ) of sieved 1912 fallout and flow deposits. For various facies listed in key, see text. Layer B_1 deposits are composite, consisting of mixed plinian and co-ignimbrite contributions; *inverted triangle* is plinian B_1 fallout, and *inverted triangle* with dot is B_1-ignimbrite. Dustfall Layers E (E) and H (H) have ≥50 wt% finer than 63 μm for all but some near-vent locations (of Layer E) that are composite flow/fall deposits (see text). Samples were sieved to 63 μm; for those with >16 wt% ash finer than sieved limit, sorting coefficients were estimated by extrapolating cumulative frequency curves (uncertainties shown by error bars). Ignimbrite field (*solid line*) after Sparks (1976) and fallout field (*dashed line*) after Walker (1971) represent data compilations for numerous other pyroclastic deposits

~30% on the dispersal axis at Katmai River, and >60% on Kodiak Island (Fig. 3). Juvenile material in Layer A is exclusively white, phenocryst-poor, high-silica-rhyolite pumice; the subsequent introduction of juvenile dacitic and andesitic material marks (by definition) the base of Layer B. The deposit is rich in lithic fragments, containing as much as 24 wt% and still having 11 wt% as far as 40 km downwind (Table 4). Exposures of Layer A at medial distances (6–13 km SE) exhibit a vague internal stratification (typically 3–5 slightly coarser intervals) not found in subsequent fallout layers, but no evidence has been found that suggests any break in deposition.

Having a pronounced ESE dispersal, Layer A was not deposited near and upwind of the vent (Fig. 5), nor has plinian rhyolite been found anywhere on the steep northern slopes of Trident (Fig. 1). The only exceptions yet found are a few centimeters of rhyolite fallout intercalated with thin rhyolite ignimbrites near the Griggs Fork (7 km, 50° from vent) and in the saddles between the peaks of Trident (5 km, 130°). Matrix-poor lenses of angular pumice clasts within rhyolitic flow deposits on the west shoulder of Mount Cerberus may also be remnants of Layer A that survived scour, but no unequivocal rhyolitic fallout has been found elsewhere north of Trident. A 1–2 cm layer of white rhyolitic ash seen locally at the base of the ignimbrite in the lower VTTS (Hildreth 1983) is not a fine-grained upwind correlative of Layer A but is now interpreted as derived from the ignimbrite itself.

Layer A is generally well-sorted ($\sigma_\phi = 0.6$ to 2.0; Fig. 6). In one of the most proximal locations sampled, 7 km S of Novarupta, Layer A is moderately well-sorted ($\sigma_\phi = 1.6$) and has a median grainsize (Md) of ~6.5 mm. The sorting is better at Kodiak, 170 km from source ($\sigma_\phi = 1$), where Md is only ~0.2 mm. Cumulative frequency curves (Fig. 7) show that as far as 36 km from source fallout Layer A contains no more than 1 wt% ash <63 μm (4φ). Average maximum pumice (MP) sizes decrease from 17 cm on the S flank of Trident (7 km), to 1.5 cm at Geographic Harbor (36 km), to 0.2 cm on the west coast of Kodiak Island (110 km from vent). Maximum lithics at those locations are 9 cm, 0.4 cm, and <0.1 cm (see Fig. 16).

Rhyolitic high-energy proximal ignimbrite (HEPI)

Within several kilometers of Novarupta, the only exposures to the base of the 1912 deposits are on wind-scoured ridgecrests where the thick mantle of dacitic plinian fallout has been stripped. At all such exposures, the basal deposits are stratified, lenticular, poorly to moderately sorted pyroclastic-flow deposits that we call 'high-energy proximal ignimbrite' (HEPI), a term we mean to be strictly descriptive. The 'high-energy' designation refers to characteristics such as wavy and lensoid bedding, scour and truncation of lower bedsets by overlying ones, sparse ballistics, and fairly good sorting ($\sigma_\phi = 1$–2) in a few of the coarser layers and lenses – features that evidently reflect high-velocity, partly turbulent, transport of fairly concentrated flows pouring over proximal ridgecrests. Although some layers have surge-like features, the HEPIs are dominantly fines-rich and

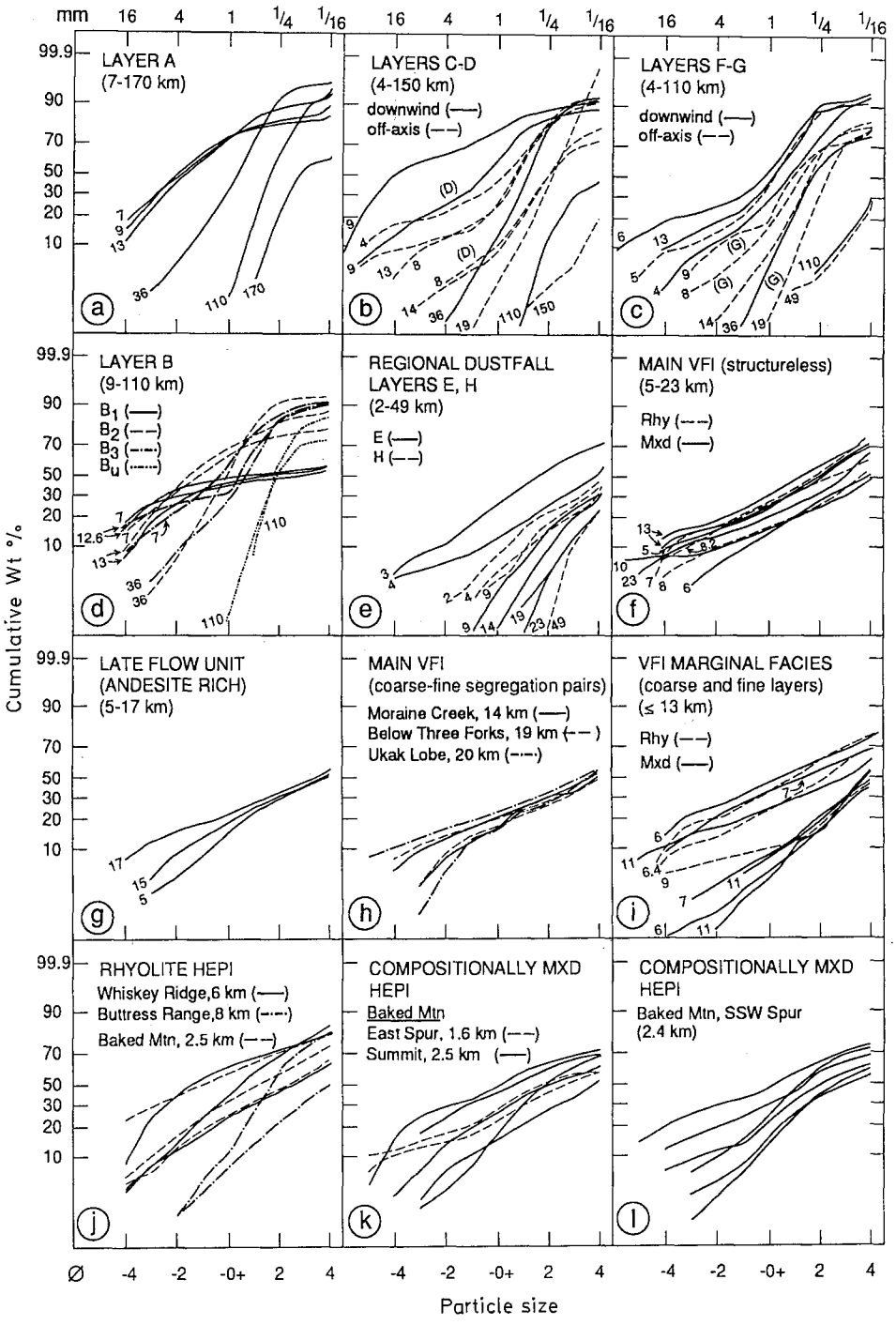

Fig. 7a–l. Size-frequency curves for 1912 ejecta, showing cumulative wt% versus particle size in phi (ϕ) units and mm. Sieve data were obtained at 1-ϕ intervals. Distance (km) from Novarupta is given for each curve. **a–d** are fallout deposits. *Curves* for Layers D and G in **b** and **c** (respectively) are individually identified; *unmarked curves* represent Layers C and F, respectively, except for undifferentiated distal deposits (36, 110 and 150 km = CD; 36, 49 and 110 km = FGH). Layers B_2 and B_3 (**d**) are plinian fall deposits, but Layer B_1 is a composite of ignimbrite ash and plinian fallout; $Bu = B_{2+3}$. Representative curves for Layer H are plotted with E (**e**) to show their similarity in grainsize distribution. Ignimbrite deposits (**f–l**) include: **f** structureless main VTTS valley-filling ignimbrite, with all-rhyolite (*rhy*) VFI and compositionally heterogeneous (*mxd*) VFI; **g** late andesite-rich emplacement unit; **h** vaguely stratified, compositionally heterogeneous, main VFI, with stratification defined by pumice-rich and pumice-poor zones (representative coarse-fine segregation pairs at locations indicated; see Fig. 1); **i** stratified marginal facies of the VFI with representative coarse and fine layers from five locations along the fringes of the ash flow sheet; **j** all-rhyolite high-energy proximal ignimbrite (*HEPI*) at locations indicated (see Fig. 1); **k, l** compositionally heterogeneous HEPI at three locations on Baked Mountain

poorly sorted ($\sigma_\phi = 2$–4; Fig. 6), and they appear to merge downslope into 'normal', unstratified, thick valley-confined ignimbrite. Similar HEPIs were emplaced throughout the ignimbrite sequence, successive bedsets reflecting the compositional zonation of the overall eruptive sequence (Fig. 4); the compositionally heterogeneous HEPIs are discussed later.

Strictly rhyolitic HEPIs are always basal, resting on pre-1912 deposits or locally (S of vent) on a few centimeters of rhyolitic fallout (Layer A). There are exposures atop Baked and Broken Mountains, Mount Cerberus, the northern spurs of Trident and Mount Katmai, Whiskey Ridge, and on the Buttress Range above the SW corner of the VTTS (Figs. 1 and 12). At a number of additional bedrock exposures, scatterings of rounded rhyolitic pumice clasts are probably lags from wind-deflated remnants of rhyolitic HEPIs that had largely been scoured away by later (heterogeneous) ash flows.

Rhyolitic HEPIs range in thickness from 5–10-cm-thick intervals interbedded with Layer A fallout in and just south of the saddles between the high peaks of Trident, to nearly 4 m atop Whiskey Ridge. Individual layers are mostly 3–30 cm thick; they are commonly inversely graded, lithic-rich (Table 4), and successive layers can have contrasting sorting characteristics (e.g., $Md_\phi = -2.5$ and 0.9, with 5 wt% and 25 wt% fine ash

≤ 63 μm, respectively, in layers at the same location atop Whiskey Ridge). Most HEPI exposures lie along unobstructed direct lines from the vent and occur as far as 9 km from source (on the Buttress Range). It is difficult to imagine that HEPIs high atop Whiskey Ridge and the Buttress Range could have been emplaced by flows that had hugged the ground prior to ascending to the crests of these steep-walled transverse ridges. Most of these deposits are thought instead to have been emplaced as ridgecapping veneers from moderately concentrated but turbulent upper parts of stratified flows that were contemporaneously producing valley-filling ignimbrite (cf. Valentine 1987; Schumacher and Schmincke 1990). They are veneers in the sense of Walker et al. (1981) in being landscape-mantling and in representing, as deposits, only a small fraction of the material that flowed past.

Rhyolitic valley-filling ignimbrite (VFI)

Exposures of fine-grained all-rhyolite ignimbrite (having few pumice lapilli >1 cm) are as thick as 13 m along the axis of the Griggs Fork (8 km NE of the vent), 4.5 m in Mageik Creek (9.5 km S of the vent), and 6 m just S of Katmai Pass (6 km from the vent). At many places in the Mageik Creek drainage (Fig. 8), the rhyolitic VFI is both underlain and overlain by several centimeters of rhyolitic fall Layer A, but the fall deposit is commonly missing at the base, a apparently scoured by the flow.

Although these are the only exposures of 100%-rhyolite valley-filling ignimbrite, such material is probably extensive beneath the upper VTTS but covered by the main compositionally heterogeneous ignimbrite. As the Griggs Fork lies along an unobstructed path from Novarupta, the rhyolitic VFI was emplaced there by direct run-out from vent; it is exposed only because its higher-energy emplacement carried it beyond the limits of the heterogeneous flows subsequently emplaced. Similarly, in Katmai Pass and Mageik Creek, exposures of all-rhyolite ignimbrite lie just outside the margins of the later, less mobile valley-filling flows. In contrast, downvalley along the axis of the VTTS, the compositionally heterogeneous ash flows (being $\sim 10\times$ more voluminous) travelled at least twice as far as the earlier, purely rhyolitic flows, which are exposed along the NE margin of the VTTS only as far as the Juhle Fork, some 9 km from the vent (Fig. 1). Farther down the VTTS, several gorges are incised to the base of the sheet, revealing only heterogeneous ignimbrite, which even at the base contains 2–10% andesite-dacite pumice clasts. Lack of incision in the upper VTTS makes our estimates very uncertain, but the volume of all-rhyolite ignimbrite is probably ~ 0.5–$1\ km^3$ and that of compositionally heterogeneous ignimbrite $\sim 10\ km^3$.

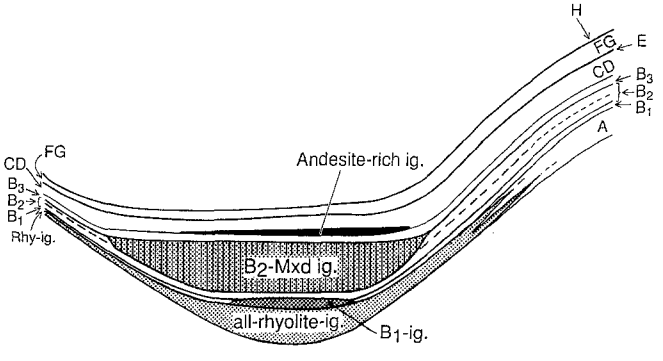

Fig. 8. Schematic sketch illustrating topographic influence of distribution of contemporaneous flows and falls. Four compositionally distinct ignimbrites (*ig*) flowed through Katmai Pass into Mageik Creek; three are compositionally equivalent to fallout Layers A (all-rhyolite ig), B_1 (B_1-ig), and B_2 (B_2-mixed ig), but there is no known plinian fall layer equivalent to the 4th (andesite-rich) ignimbrite. For description of facies, see text

Rhyolitic ignimbrite marginal fringe. In contrast to the main, compositionally heterogeneous ash flows (which outside the near-vent region were strictly valley-confined), the earlier, more energetic, rhyolitic ash flows swept far up the enclosing slopes. Massive or crudely stratified, pinkish deposits of purely rhyolitic ignimbrite on the S and SE flanks of Mount Griggs (Fig. 1) form a run-up fringe adjacent to the thick axial ignimbrite along the Griggs Fork. Here, the ignimbrite wedges out gradually from as thick as 13 m along the stream axis to only a few centimeters at distances of 1–2 km upslope. A continuous thin fringe of pinkish ignimbrite also extends across the SW slope of Mount Griggs at elevations as much as 450 m higher than the adjacent VTTS floor along Knife Creek; across-slope transport of a somewhat less concentrated upper part of the ash flow is suggested here by charred and flattened 1912 willows aligned in that direction. Similar ignimbrite as far as 1.5 km up the Juhle Fork side canyon, just beyond Mount Griggs and ~ 9 km from vent, is up to 1 m but generally <40 cm thick. Snowmelt on the steep slopes of Mount Griggs caused local remobilization of this rhyolitic ignimbrite fringe, producing many small, gulch-confined, all-rhyolite debris flows that underlie and interfinger with the subsequently emplaced dacite-fall units on the lower flanks of the volcano.

A comparable thin fringe of rhyolitic ignimbrite, typically 5–20 cm thick and commonly vaguely stratified, mantles lava-flow benches along the eastern base of Mount Mageik. These deposits are best preserved on the benches adjacent to but up to 250 m higher than the valley-confined ignimbrite along Mageik Creek, and in places they can be traced downslope and shown to merge with the 4-m-thick rhyolitic ignimbrite along the valley axis (Fig. 8).

A few centimeters of fine rhyolitic ash (or locally just ash filling cracks in bedrock) is preserved beneath Layer A fallout on Observation Mountain and on the lower southern slopes of Trident. This probable ash-cloud deposit suggests that at least one small ash flow came down Mageik Creek before deposition of any Layer A plinian material at the SW edge of its fallout sector. Similar basal ash (white, light-grey, or pale lavender) is present along the crest of the Buttress Range as far as 15 km NW of Novarupta, where it is as thick as 10 cm

and contains scattered rhyolitic pumice granules, and on the cross-valley moraine near Three Forks, where it is only 1–2 cm thick.

Both the marginal-fringe deposits and rhyolitic HEPI, 2–9 km from vent, have wide ranges of sorting ($\sigma_\phi = 1$–3) and of fine-ash content (4–30 wt% < 63 μm), but most layers and lenses in these deposits are poorly sorted and fines-rich like the rhyolitic valley-confined ignimbrites nearby (Figs. 6 and 7).

Time relationships and emplacement mechanisms

The western edge of the Layer A fallout sector is abrupt (Fig. 5), and the rhyolite ash flows that penetrated Katmai Pass barely overlapped with it spatially. Nonetheless, intercalation of plinian Layer A with all-rhyolite flow deposits along Mageik Creek and in the saddles along the crest of Trident unambiguously establishes the contemporaneity of flow and fall emplacement. Topography strongly influenced pyroclastic-flow emplacement, and, at locations not reached by flows, Layer A forms a continuous nongraded but vaguely stratified plinian deposit.

The relative distribution of the rhyolitic falls and flows also indicates their synchroneity. At many locations where all-rhyolite flows are exposed, plinian Layer A is scoured or is only partially preserved as intercalations of fallout between thin ignimbrite flow units. The fact that unbroken Layer A fallout is as thick as ~1.4 m just south of Trident (above or beyond the flows), but absent on the north flank of Trident, suggests that it was either scoured or unable to accumulate (owing to synchronous HEPI emplacement) on the vent-facing northerly slopes.

Distribution of the all-rhyolite HEPIs and marginal-fringe deposits relative to rhyolitic valley-filling ignimbrite indicates that they are all depositional facies that resulted from the same event. Respectively, the HEPI and marginal-fringe deposits are thought to be proximal and medial-to-distal equivalents, both deposited from less-concentrated upper parts of stratified flows (cf. Valentine 1987) that graded down into volumetrically dominant, high-particle-concentration zones that concurrently produced the valley-filling ignimbrites (Fig. 9). Both HEPI and marginal-fringe facies were deposited on high ground adjacent to valley-confined ignimbrites of similar (all-rhyolite) composition and of comparable mean grainsize and lithic contents (Fig. 6, Table 4). At elevations only a few hundred meters above the valley floors, the density-stratified flows need have been neither very dilute nor strongly turbulent – just slightly more dilute and turbulent than down near the valley bottom. On proximal ridgecrests and on valley-margin lava-flow aprons, basal turbulence was probably enhanced by passage over rough topography, favoring local sorting and stratification. At medial locations (Mageik, Griggs), the thin marginal-fringe deposits that taper out upslope from the valley-confined ignimbrite are similar, at least conceptually, to the 'overbank deposits' of Schumacher and Schmincke (1990). At distal locations (Buttress Range, Three Forks moraine, Observation Mountain), the thin rhyolitic ash layers were probably deposited by truly turbulent ash clouds that detached and continued beyond the termini of valley-confined flow units.

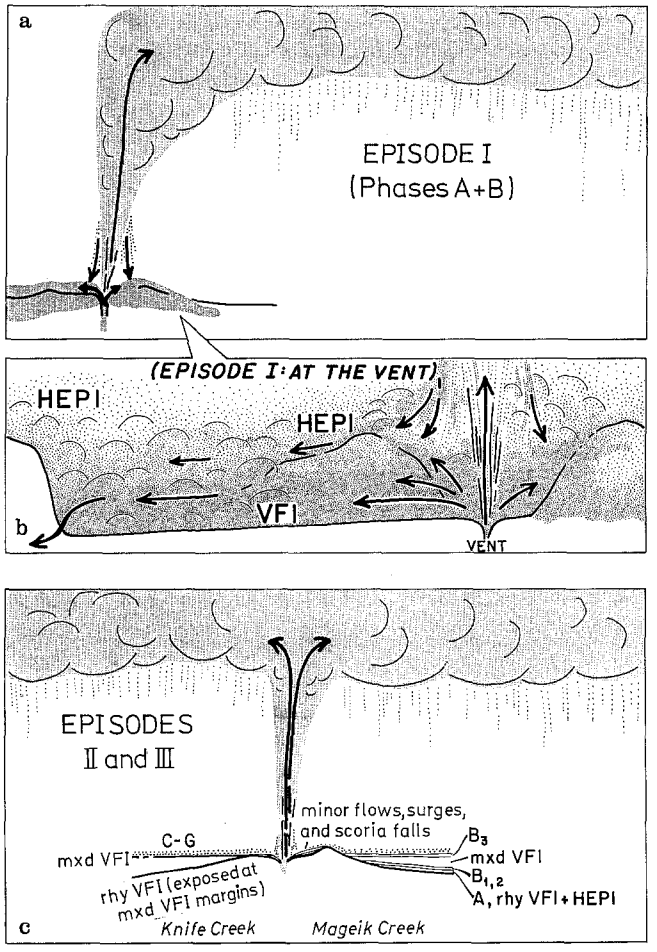

Fig. 9a–c. Cartoon illustrating processes that emplaced the proximal deposits shown in Fig. 4. **a** Compositionally zoned SE-directed plinian fallout was emplaced contemporaneously with similarly zoned ignimbrite during Episode I. Plinian Layers A and B were deposited downwind on and beyond Trident, but almost none was deposited in the VTTS. Although most of the ignimbrite filled the VTTS, smaller tongues compositionally equivalent to A, B_1, and B_2 did go through Katmai Pass into Mageik Creek; plinian fallout B_3 accumulated to the south while contemporaneous ignimbrite filled the VTTS, but no fallout accumulated contemporaneous with final valley-filling ash flows, which were andesite-rich. **b** Schematic proximal sketch of Episode I showing HEPI-emplacement on ridges above the valley floor from moderately turbulent (but still concentrated) upper zones of density-stratified ash flows that concurrently were depositing VFI just downslope. Near-vent Baked and Falling Mountains (schematically drawn) were overrun by these flows; Whiskey Ridge (represented on far left) blocked and diverted the denser lower part of the flows (VFI), while HEPI deposits accumulated on the top of the ridge several hundred meters higher. Marginal column sloughing, vent-clearing outbursts, and high-energy turbulent outflow all contributed to complex near-vent stratigraphy. **c** Episodes II and III were dominantly plinian, largely dacite, and distributed Layers C–G both N and S of vent; minor flows and surges in the near-vent region combined with scoria-rich fallout to make composite flow-fall lenses intercalated with the dacite plinian layers proximally

Synchroneity of HEPI, VFI and plinian emplacement means that different eruptive processes were occurring simultaneously (Fig. 9): (1) a convecting plinian column produced regionally distributed fallout; the deposit shows minor fluctuations in grainsize but concurrent generation of ash flows never fully interrupted the column; (2) voluminous density-stratified ash flows gushed directly away from vent, undergoing little or no ascent with the coexisting plinian column; deposits are the rhyolitic VFI, its marginal fringe facies, and most HEPI; and (3) ash flows that sloughed off the margins of the plinian column from modest elevations (<1 km?) may also have contributed to the ridgecrest HEPI veneers, but most such material drained off to merge with the main VFI.

Eruptive Episode I (Phase B)

Redefinition of 'Layer B'

As originally defined by Curtis (1968), Layer B in upper Knife Creek 'is composed almost entirely of very fine-grained pink ash', of which 50% is finer than 63 μm (Fig. 7i, ignimbrite marginal facies). Heavy-liquid separations show it to consist there of ~95 wt% glass, including spherical bubble shards (Fig. 5-12 of Fisher and Schmincke 1984) unique to the rhyolitic eruptive episode, and 2–5% each of phenocrysts and lithic ash (Hildreth 1983). The distinctive mineralogy of the different 1912 pumice types permits the calculation that as many as 20% of the phenocrysts at Curtis' type locality were derived from andesitic and dacitic pumice (Hildreth 1983). Curtis (1968) observed that the deposit thins away from the main ignimbrite and 'is closely related to the tuff flow and represents either the ash cloud that accompanied it or the ash left behind as the tuff flow receded from its highest levels'. Hildreth (1983) suggested deposition by marginal surging during VFI emplacement. Further fieldwork has strengthened our view that what Curtis called Layer B is a marginal facies of the main heterogeneous ignimbrite and that it is part of the vaguely stratified valley-marginal fringe (Fig. 7i) that consists largely of the all-rhyolite marginal facies described earlier. We thus refer to these fringing wedges of pyroclastic-flow material as ignimbrite marginal facies, and we redefine and restrict the term Layer B to plinian *fallout* that accompanied emplacement of compositionally heterogeneous ash flows.

Plinian Layer B

We divide Layer B into three subunits on the basis of composition and grainsize, even though no depositional break has been recognized within Layer B (or between it and Layer A). Like Layer A, all three subunits are largely confined to a 90° sector SE of vent (Fig. 5), except that the last (B_3) also occurs (thinly) as far as 8 km W and 9 km N of Novarupta. The compositional progression within Layer B, from rhyolite-dominant to rhyolite-poor, parallels that in the contemporaneously emplaced succession of ignimbrites. Ignimbrite-derived oxidized fine ash is abundant in Layer B_1 and sparsely but prominently coats fallout lapilli in the upper parts of B_2 and B_3, providing a series of distinctively colored, terra-cotta to burnt-orange markers.

Although its coarse ash and lapilli fractions show little or no grainsize difference from subjacent Layer A, fall Layer B_1 is distinctive in containing up to 35 wt% fine co-ignimbrite ash, which imparts a prominent terra-cotta color that contrasts with the white fines-poor lapilli-rich fallout above and below. Toward the axis of Mageik Creek and in nearby swales, the B_1 fall layer grades laterally into a true ignimbrite flow unit as much as 21 cm thick (Fig. 8), but upslope the fraction of fine ash lessens. Within a few kilometers of axial Mageik Creek and as far east as Katmai River, the fines-rich interval defined as Layer B_1 is characteristically 3–8 cm thick (Fig. 3), but it thins laterally away from the valley-confined ignimbrite and is absent above an elevation of ~1000 m on the south slopes of Mount Katmai. Because of its intimate genetic relationship with the Mageik Creek ignimbrite, Layer B_1 can be identified only as far as 13 km SE of vent. Compared to Layer A at given locations, Layer B_1 is very poorly sorted ($\sigma_\phi > 4$) and finer grained (Figs. 6 and 7), owing almost entirely to 'contamination' by the co-ignimbrite ash contribution.

Layer B_1 and the contemporaneous ignimbrite that provided its fine-ash component were the earliest emplacement units to contain any andesitic and dacitic pumice clasts. Near Mageik Creek and Katmai River, the pumice in B_1 fallout is 82–99% rhyolitic (Table 2), just as in the associated Mageik Creek ignimbrite and in the far more voluminous flow units that were the first to reach the lowermost VTTS.

Layer B_2 is a compositionally mixed fall unit that shows slight inverse grading and parallels the VTTS ignimbrite sequence in having 51–93% rhyolitic clasts in its lower half, grading up to as much as 60% dacitic and andesitic clasts at its top. It is as thick as 50 cm high on Trident ~5 km SE of source, and it characteristically has a burnt-orange top imparted by a small amount of oxidized dacitic and andesitic ash that coats individual lapilli. At the southern base of Trident (~8.5 km SSE of source) Layer B_2 is up to 30 cm thick, but it is only partly intact (variably 4–23 cm) along the nearby axis of Mageik Creek where it was shaved by and directly underlies 8 m of heterogeneous valley-filling ignimbrite (Fig. 3; section 5).

In distal fall sections along the NW coast of Shelikof Strait, the lower part of Layer B can be distinguished from white Layer A beneath it by a pink tinge caused by a little oxidized ash adhering to the pumice clasts. Clast compositions of fall layers (Table 2) at Geographic Harbor (36 km SE of source) confirm that the basal white fallout is 100% rhyolite (Layer A) and that the overlying pink fallout, ~24 cm thick and containing nearly 10% intermediate clasts, correlates compositionally with the lapilli fraction of Layer B_1 and with the bottom half of B_2 as seen near Mageik Creek. Although the B_1 co-ignimbrite ash component is trivial or absent so far from

source (Fig. 3), the upward change in rhyolite-dacite clast proportions is similar all the way to Geographic Harbor and even as far away as Kodiak Island (Tables 2 and 3).

Layer B_3 extends the compositional zoning trend of Layers A-B_1-B_2, containing pumice that is 20–38% rhyolite and 59–76% dacite at its base (similar to the top of B_2) but only 11–25% rhyolite and 75–87% dacite at its top; clast counts also gave 0–6% andesitic scoria (Table 2). We separate Layer B_3 from Layer B_2 because its base is slightly finer grained than the top of B_2 and because it tends throughout to contain a dusting of oxidized (burnt-orange) ash, though (as in B_2) this is most prominent at its top. On the southern slopes of Trident and Mount Katmai, Layer B_3 is 37–57 cm thick and is coarsest (MP = 6–16 cm) in its middle portion. The pumice-clast compositional proportions just given for Layer B_3 are comparable to those in some relatively late (but not the final) ignimbrite flow units in the VTTS (Table 2), none of which penetrated Katmai Pass.

Unlike Layers A, B_1 and B_2, Layer B_3 is also distributed (thinly) outside its main SE dispersal sector. Exposures of heterogeneous fallout containing only 20–30% rhyolite occur beneath Layer C on Broken Mountain and the Buttress Range (Table 2; sections 42 and 56) and atop rhyolite-rich ignimbrite on the lower slopes of Mount Griggs (section 44). Along Mageik Creek, Layer B_3 is sandwiched between thick Layer C and heterogenous VFI, which replaces compositionally equivalent Layer B_2 near the drainage axis (Figs. 3 and 8). Wherever still-later rhyolite-poor ignimbrite flow units are present, as throughout the VTTS, compositionally equivalent Layer B_3 is absent.

Outside the Mageik Creek drainage basin, the co-ignimbrite ash that defines Layer B_1 is absent, and the base of B is defined by the first occurrence of dacitic or andesitic pumice. Layers B_2 and B_3 are still distinct as far as Geographic Harbor (36 km downwind), but are generally hard to separate beyond ~15 km from source in off-axis locations, because color and grainsize become gradational as the unit fines and thins. The compositional zonation within a unitary Layer B persists, however, even to Kodiak Island (Fig. 3; sections 8 and 9).

Compositionally heterogeneous (main) valley-filling ignimbrite (VFI)

Most of the exposed ignimbrite is compositonally mixed, containing various proportions of rhyolite, dacite, and andesite pumice, and it is nearly structureless except for internal laminar shear segregations (pseudo-flow units) a few centimeters to several meters thick near margins and termini (Fig. 10). Because *persistent* interflow partings have not been seen on gorge walls in medial parts of the main ignimbrite, it is thought that as much as 90% of the exposed sheet was emplaced quasi-continuously in the VTTS. One compositionally heterogeneous flow unit penetrated Katmai Pass (Table 2) and left a structureless deposit up to 20 m thick along Mageik Creek. A few late flow units, none more than a few meters thick, are present both proximally and distally, and axially some occupy shallow swales that formed by drainaway or compaction of earlier ignimbrite. These include dark-matrix andesite-rich units that contrast sharply with underlying light-colored rhyolite-rich ignimbrite. The andesite-rich flow units were generally the least mobile, being limited mostly to the upper half of the VTTS, but one reached Three Forks, 17 km from the vent (Fig. 1); another flowed through Katmai Pass, feathering out beyond the Pass ~3 km down the Pacific slope. Having higher magmatic *and* emplacement temperatures than the earlier flows, these andesite-rich units are sintered or partly welded in much of the upper VTTS. The absence of co-ignimbrite ash or other fall deposits between flow units and the scarcity of erosive channeling between them imply that the flows were emplaced in close temporal succession. Local cross-bedding due to wind-reworking or surges near West Mageik Lake and shallow erosional swales between flows near Three Forks do, however, suggest a break of minutes to hours prior to emplacement of the andesite-rich flow units, which were the final products of Episode I.

A few flow units (e.g., the dark andesite-rich flows) are unequivocally vent-derived, but the general distinction between such flows and secondary units produced by flow budding, internal shear, and different flow paths around obstacles, is still under study. Despite good exposure on the walls of longitudinal gorges, pumice- and lithic-concentration zones in the main ignimbrite generally persist for only tens of meters and provide only vague, discontinuous stratification within an otherwise mostly structureless deposit. Nonetheless, field counts of pumice-clast proportions on gorge walls permit delineation of compositionally different sets of flows or pulses and even of compositional zoning within some apparently structureless sections 20–30 mm thick. Clast proportions range widely, from 90–99% rhyolitic pumice clasts near Three Forks, in the distal Ukak lobe, and deep in the Juhle Fork in the central VTTS – to as few as 1–2% rhyolitic clasts in late-emplaced flows that make up the top several meters of the ignimbrite in the upper VTTS. Pumice counts also establish that (except for the all-rhyolite upper-VTTS fringe previously described) all of the rhyolite-rich VFI now exposed in the mid-to-lower VTTS contains at least a little dacite and andesite, with increasing amounts of dacitic, andesitic and banded pumice incorporated upward in the deposit (Table 1 of Hildreth 1983). The all-rhyolite ignimbrite exposed in Katmai Pass, Mageik Creek, and around Mount Griggs belongs to the earlier rhyolitic Phase A; all its exposures lie within ~10 km of Novarupta and are restricted to the periphery of the main (Phase B) ignimbrite, which it presumably also underlies in the upper VTTS. Four flows crossed Katmai Pass: the first all-rhyolite, the second rhyolite-dominant (B_1 ignimbrite, 98–90% rhyolite), the third (and thickest) ~50/50 rhyolite-dacite, and the fourth rich in andesite but poor in rhyolite.

Grainsize and sorting in the main VFI are comparable to those in many other ignimbrites (Figs. 6 and 7). Concentration of our main-VFI data in the finer-grained

half of the pyroclastic-flow field in Fig. 6 largely reflects our failure (under field conditions at Katmai) to collect bulk samples of coarser zones. Among main-VFI samples sieved to date, 10–30 wt% is <63 μm and 60–80 wt% is <1 mm (Fig. 7); lithic content ranges from 1–6 wt% and free crystals from 2–31 wt% (Table 4). Variability in crystal content within ignimbrites can be caused by elutriation of fine ash and gravitational sorting during outflow (Sparks and Walker 1977), but at the VTTS it also reflects progressive increases in proportions of phenocryst-rich dacitic and andesitic pumice at the expense of phenocryst-poor rhyolite in the zoned sheet.

Pseudo-flow-units. Internal sorting of pumice clasts locally defines vague discontinuous stratification (typically on a thickness scale of decimeters to a few meters but in places as thin as 1–5 cm), principally near the margins and termini of the main ignimbrite (Fig. 10). Inverse grading of pumice clasts is typical where coarse-fine pairs (Fig. 10a) are well defined, but more commonly sharp boundaries are lacking, and pumice-rich zones are gradational upward and downward with pumice-poor zones. Lithics are not conspicuously graded. Grainsize data for coarse-fine pairs are plotted on cumulative frequency curves in Fig. 7. Convergence of these curves between $+1_\phi$ and $+2_\phi$ (1/2 to 1/4 mm) indicates that 50–60% of the ash flow particles are unaffected by the sorting processes that developed the pumice-rich and pumice-poor zones. Such coarse-tail grading of pumice clasts is common within many ignimbrite flow units

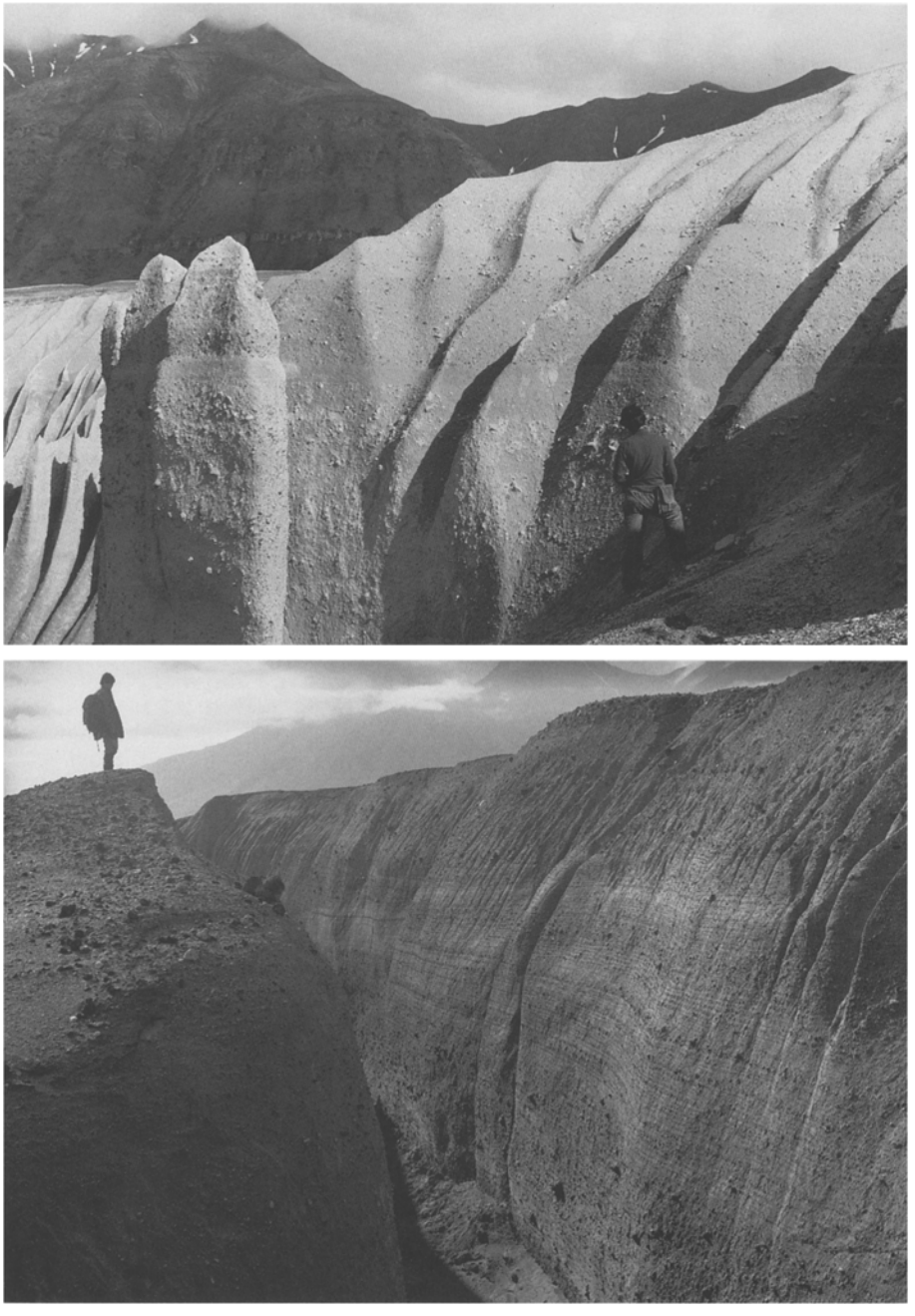

Fig. 10. a Example of 1–3-m-thick segregations (secondary flow units) that commonly develop near distal margins of otherwise almost structureless, main VTTS ignimbrite; location is on NE side of Ukak River 2 km downstream from Three Forks, 17 km from vent. **b** Strongly developed 1–10-cm-thick laminations in the ignimbrite 15 km from vent and ~1.5 km upstream from the cross-valley moraine (Fig. 1)

(Sparks 1976). The segregations are also similar to true vent-derived flow units in that some have fine-grained basal layers.

The segregations apparently developed as each thick ash flow slowed to a halt, presumably from its base upward, engendering internal velocity gradients and consequent internal shear. The stratification is thus a locally developed feature and does not reflect flow units that originated at the vent. As such pseudo-flow-units only developed very late during emplacement of the ash flows, this style of plane-parallel but discontinuous stratification is strikingly different from the turbulence-induced lenticular layering of the near-vent HEPI veneers. In the lower VTTS, 15 km from source and just above the cross-valley moraine (Figs. 1 and 11) that diverted the ignimbrite (Hildreth 1983), such stratification is strikingly well-developed; the downflow change from homogeneous, unstructured tuff to a stratified deposit having as many as 100 segregated layers (Fig. 10b) occurs within 200 m. The change in flow direction imposed by the moraine may have especially enhanced internal shear in the already slow-moving flow at this location.

Heterogeneous high-energy proximal ignimbrite (HEPI)

Stratified ignimbrite showing wide ranges in grainsize, sorting, and (rhyolite/dacite/andesite) pumice ratios (Table 2) mantles the rugged topography around the perimeter of the Novarupta depression (Figs. 1 and 12). These compositionally zoned, generally oxidized, layered deposits are exposed beneath the dacite fallout

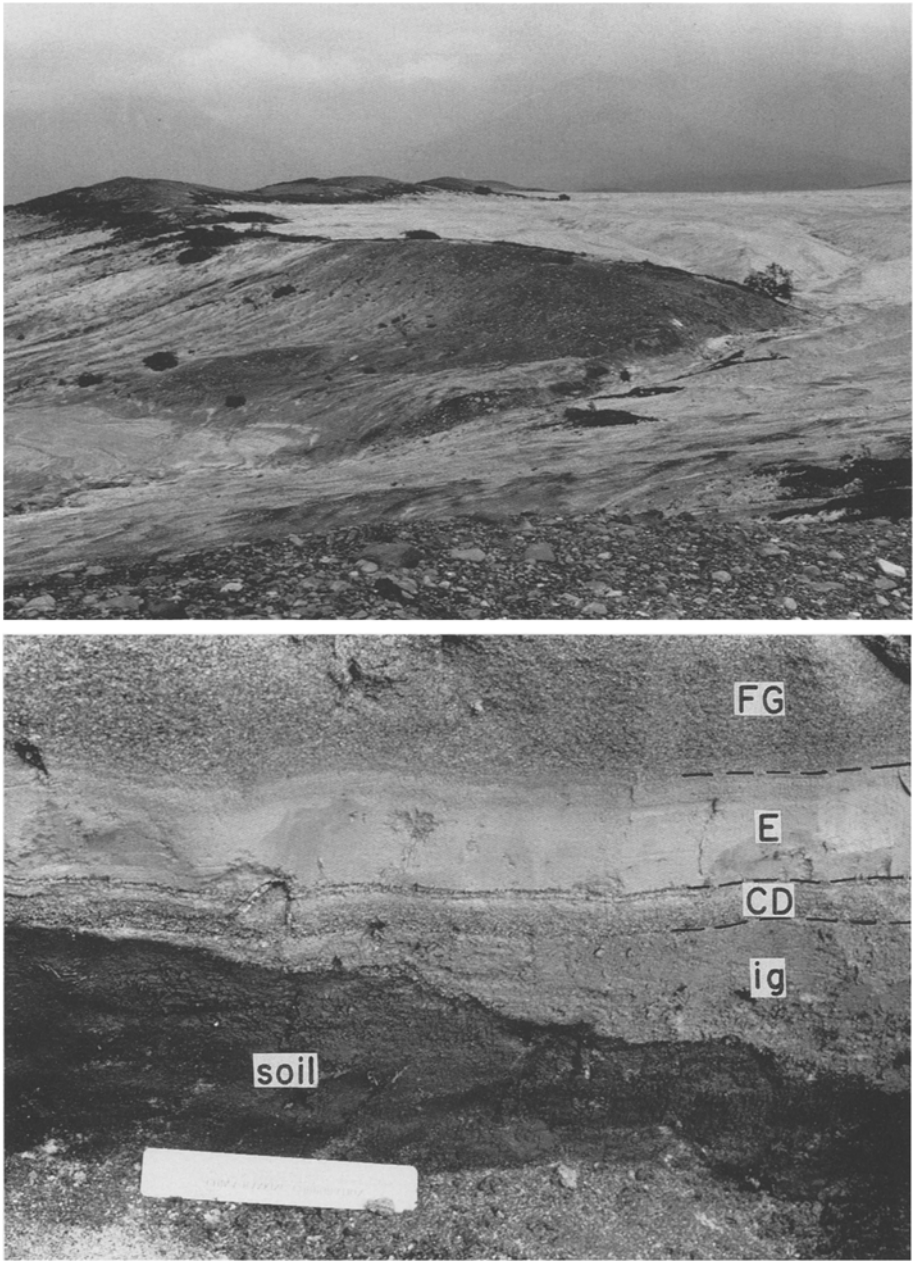

Fig. 11. a Ignimbrite banked against cross-valley moraine in the VTTS, 16 km from source, ENE of Three Forks (Fig. 1). **b** Edge of ignimbrite (*ig*) where it wedges out against moraine. Plinian deposit *CD*, Layer *E*, and plinian deposit *FG* overlie the ash flow. *Ruler* is 15 cm long

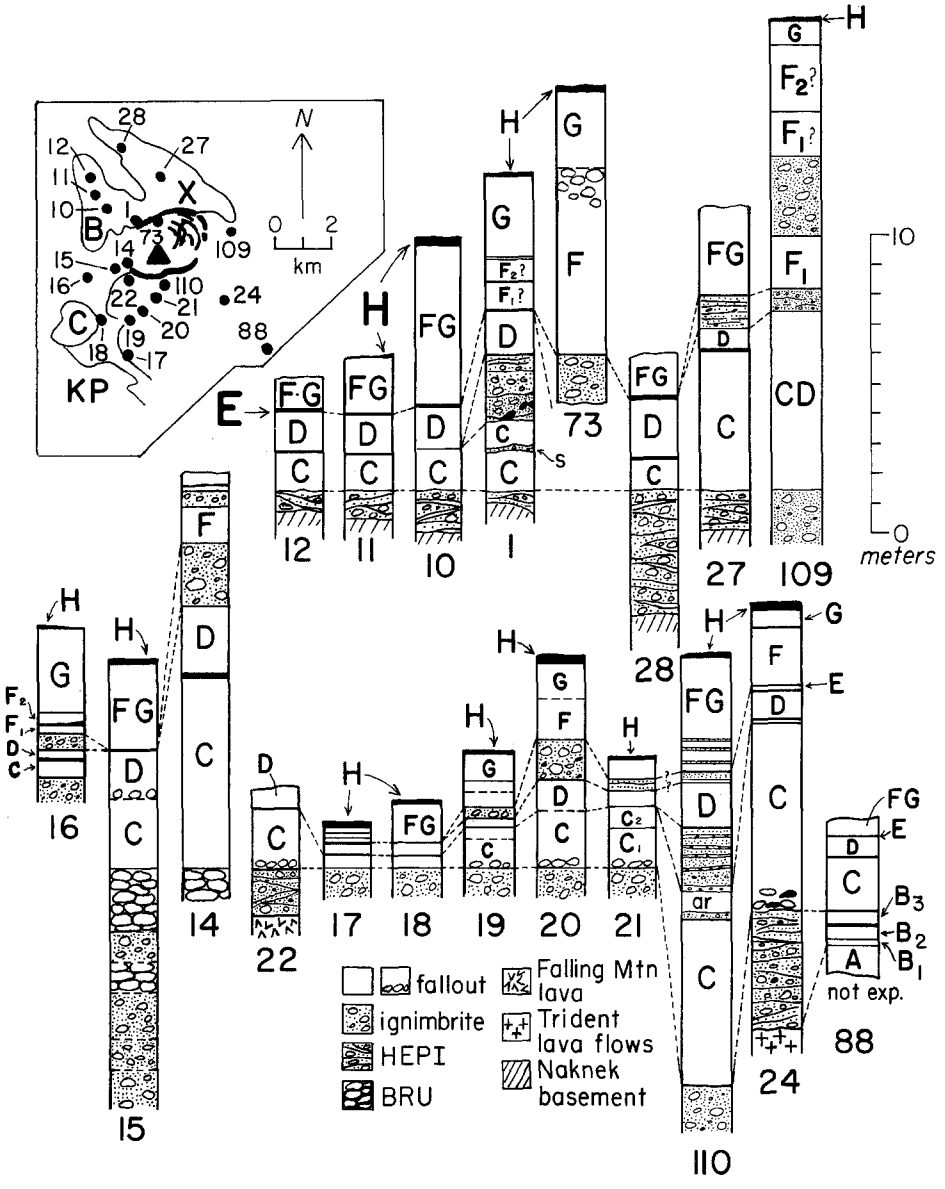

Fig. 12. Sections of proximal flow and fall deposits, located on inset map of near-vent area, on which heavy lines are vent-surrounding scarps and fractures. Layers A–H are labelled; other patterns are explained on the diagram. *Open shapes* (pumice) and *filled shapes* (lithics) suggest relative sizes or distinctive deposit features (sections 73 and 24) and are not drawn to scale. Although widely scoured proximally, all-rhyolite HEPI is preserved beneath compositionally mixed HEPI at the bases of sections 10 and 28. The block-rich flow units (*BRU*, sections 14 and 15) associated with Layer C, intraplinian ash flows within the C–D and F–G fallout, and ultra-proximal andesite-rich fallout ('*ar*' in section 110), are largely confined to Novarupta basin. Interplinian events that occurred during the 'E' hiatus sent flow deposits down the gulch south of Falling Mountain (sections 19, 20, 21 and 110) and over Broken Mountain (section 27), and they are also exposed near Novarupta (sections 14 and 109)

on the windswept ridges of Trident, Falling Mountain, Mount Cerberus, the NW flank of Mount Mageik, on Whiskey Ridge, and on all spurs of Baked and Broken Mountains; they rest either on bedrock or on the rhyolitic HEPI previously described.

Most exposures are 0.5–5 m thick and consist of ~5 to 25 discrete layers, individually 1–35 cm (mostly 3–15 cm) thick. Alternating layers are either (1) fines-rich and matrix-supported; (2) dominantly coarse-to-medium ash and pumice granules; or (3) clast-supported beds rich in pumice lapilli. The variance in Md_ϕ, σ_ϕ, lithic content (0.6–16 wt%), and fine ash content (<10 to ~50 wt% <63 μm) is great even among successive beds at given outcrops; some data are given in Table 4 and Figs. 6 and 7, but the coarsest layers (rich in pumice blocks) have not been sampled. Most layers are apparently planar or gently undulating but, as many pinch out within 5–15 m laterally, they are actually lenticular at outcrop scale. Many show coarse-tail inverse grading of pumice, but only a few have any internal cross-bedding (generally vague and low-angle in sandy layers). No accretionary lapilli or other signs of involvement of external water have been noted.

The two thickest (10–15 m) HEPI sections are also the coarsest, containing abundant pumice and lithic blocks: (1) on the SSW spur of Baked Mountain (~2.5 km west of Novarupta), >110 HEPI layers (each 1–30 cm thick) are stacked on a flat-topped ridgecrest ~200 m above the valley floor and directly athwart the main exit from Novarupta basin; (2) on the east shoulder of Falling Mountain, only ~1 km from Novarupta, ~15 alternately fines-rich and lapilli-rich HEPI layers make up a 2-m basal section that is overlain by ~11 m of more massive ignimbrite, consisting of at least five rhyolite-poor emplacement units plastered against the steep vent-facing wall.

Successive pulses commonly scoured earlier HEPI layers, leaving numerous internal unconformities, but where early strata are partly intact, the basal layers are the lithic-richer all-rhyolite HEPI. The more volumi-

nous compositionally mixed HEPI show quite variable pumice proportions, having as much as 90% dacitic or up to 35% andesitic pumice (Table 2). The gross upward compositional sequence thus parallels that of the VFI and of fallout Layers A–B. Also in common with the VFI, the compositionally mixed HEPI were less vigorously mobile than their rhyolitic predecessors; they failed to reach the crest of the Buttress Range or to run far up the aprons of Griggs and Mageik, and they are much thinner than the underlying rhyolitic HEPI atop Mount Cerberus and Whiskey Ridge.

As already discussed for Phase-A rhyolitic HEPI, we favor emplacement on ridges above the valley floor from the moderately turbulent but nonetheless still quite concentrated upper zones of density-stratified ash flows (Fig. 9) that concurrently were depositing poorly sorted VFI only a few hundred meters downslope. Stratification-inducing turbulence may have been enhanced by (1) topographic roughness, (2) virtual hydraulic jumps over ridgecrests, and (3) in ultra-proximal locations, by being still within the deflation zone of collapsing flows, consistent with a small ballistic contribution locally.

Wedge edge and low-energy emplacement of main VFI

In contrast to the relatively high-energy emplacement conditions within a few kilometers of vent, and in contrast to the extensive marginal fringe of the earlier all-rhyolite ignimbrite, relations along the medial and distal margins of the heterogeneous VFI show evidence for well-confined emplacement of the main mass of the VTTS ignimbrite. The ignimbrite wedges out distally against obstructions that were essentially perpendicular to the direction of flow at the SE base of Overlook Hill, along the N base of Mount Katolinat, and against the cross-valley moraine 16 km from source (Fig. 11). Although ash flows crossed through saddles in this low moraine (Hildreth 1983), they generally wedged out against it and failed to run up it significantly. Where the ignimbrite banks against the moraine, it commonly pinches out at elevations only ~2 m higher than its adjacent valley-floor surface. In the Windy Creek embayment (Fig. 1) the ignimbrite remains virtually horizontal right up to its confining margins, where it either banked flush against higher walls or barely spilled over lower ones to form thin overbank sheets. The ash flows filling the old gorge of Windy Creek were so sluggish that they charred but failed to strip the turf from sidewalls as steep as 38°.

At the base of steep valley walls that laterally confine medial heterogeneous ignimbrite in the VTTS and along Mageik Creek, marginal wedges feather out several meters to tens of meters above the general level, resembling the valley-margin structures in fine-grained flow units illustrated by Freundt and Schmincke (1986; their Fig. 12b). Along the side of the Buttress Range 12 km from source where the floor of the VTTS narrows from 7 to 3 km wide, such a wedge reaches >50 m above the main flow surface (location LH on Fig. 1). Hildreth (1983) suggested that this may have been due to temporary local elevation of the flow where the VTTS narrows to its minimum width. We have now recognized, however, that this ignimbrite wedge is distinctive in its composition (rhyolite-plus-andesite) and that it was part of a late flow sequence that came down Knife Creek. After clearing Broken Mountain, the flow spread across valley, and the relatively high-reaching marginal wedge appears simply to have been a WNW-moving oblique run-up against the Buttress Range.

Falls and flows: time relationships

Eyewitness reports (Martin 1913; Griggs 1922) of three discrete episodes of fallout at Kodiak village constrains eruption of the ash flow sheet to a maximum interval of ~18 h (Hildreth 1983, 1991), although actual emplacement time could have been shorter and/or episodic. Microprobe analyses of glass shards (Table 3a) and stratigraphy on both sides of Shelikof Strait (Fig. 3) show that ~75% of the total fallout at Kodiak, including part of the brown ash that Martin had assigned to the second period of ashfall, actually erupted during Episode I.

Three considerations constrain the time-emplacement relationships between the falls and flows erupted during Episode I: (1) changes in clast proportions in the fallout are parallel to the compositional variation in the ignimbrite; (2) the compositionally zoned fallout sequence (A through B_3) was emplaced continuously from a fluctuating but essentially uninterrupted plinian column; (3) flows and falls of similar composition are intercalated with one another on Trident, near Katmai Pass, and along Mageik Creek. These relations are not seen in the VTTS because the A–B fallout was strongly directed to the SE and because the ash flows in the VTTS scoured away any contemporaneous proximal fallout. Thus, even though we have recognized at least seven compositionally distinct ash flow sequences in the VTTS, the time relations between flows and falls are best demonstrated by the four flows that crossed Katmai Pass (Fig. 8).

Of the four ash flows that crossed Katmai Pass, three have pumice proportions that are equivalent to specific intervals of plinian fallout. The initial all-rhyolite VFI is compositionally equivalent fo fall Layer A, with which it is intercalated. The subsequent small-volume rhyolite-dominant B_1 ignimbrite is compositionally similar to fall Layer B_1 and the bottom half of Layer B_2; it actually grades laterally into fall Layer B_1 adjacent to Mageik Creek (Fig. 8). No further ash flows crossed Katmai Pass until the supply of dacitic magma to the vent was amply established. The third flow to penetrate the Pass deposited a 20-m-thick valley-filling ignimbrite that has subequal proportions of both rhyolite and dacite. It overlies the lower part of fall Layer B_2 along Mageik Creek (Figs. 3 and 8) and is compositionally similar to the upper one-third of Layer B_2. Preservation of rhyolite-rich Layer B_1 and ~2/3 of Layer B_2 directly beneath this ignimbrite along the axis of Mageik Creek shows that the voluminous VTTS ash flows compositionally and temporally equivalent to those fall intervals were restricted to the northern side of Katmai Pass. Dacite-rich flows compositionally correlative to fall layer B_3 are

likewise found only north of Katmai Pass. The fourth flow unit that crossed the Pass is part of a set of andesite-rich ash flows that caps the ignimbrite sequence in the upper VTTS (Figs. 4 and 7) but has no widespread compositionally correlative fall layer, apparently reflecting relatively low fountaining that fed these partially welded, scoria-rich flow units. This indicates that eruption of Phase B plinian fallout was over by the time these final, nearly rhyolite-free, andesite-rich ash flows were emplaced.

Intercalation of zoned sequences of compositionally similar plinian falls and ignimbrites along Mageik Creek and near Katmai Pass (Fig. 3; section 4) unequivocally demonstrates their contemporaneity. Although only parts of the compositionally zoned ignimbrite sequence crossed the Pass, the much more voluminous deposit on the VTTS side of the Pass shows no evidence of any significant break in ash flow emplacement succession until just before the andesite-rich flow units that cap the Episode I sequence. Similarly, south of Katmai Pass and Trident, wherever protected from ignimbrite scour, the zoned A–B plinian fallout sequence accumulated without any identifiable interruption. Although contaminated intermittently by pulses of co-ignimbrite fine ash (which defines B_1 and the tops of B_2 and B_3), the A–B fallout on the south flanks of Trident and Mount Katmai represents both an unbroken compositional succession toward a progressively smaller fraction of rhyolitic ejecta and a physically uninterrupted plinian lapilli-fall deposit. There are slight fluctuations in grainsize within the unit, but neither within the all-rhyolitic part designated Layer A nor within the zoned part called Layer B is there any interval of significant normal grading that could reflect a hiatus in plinian activity. In contrast,

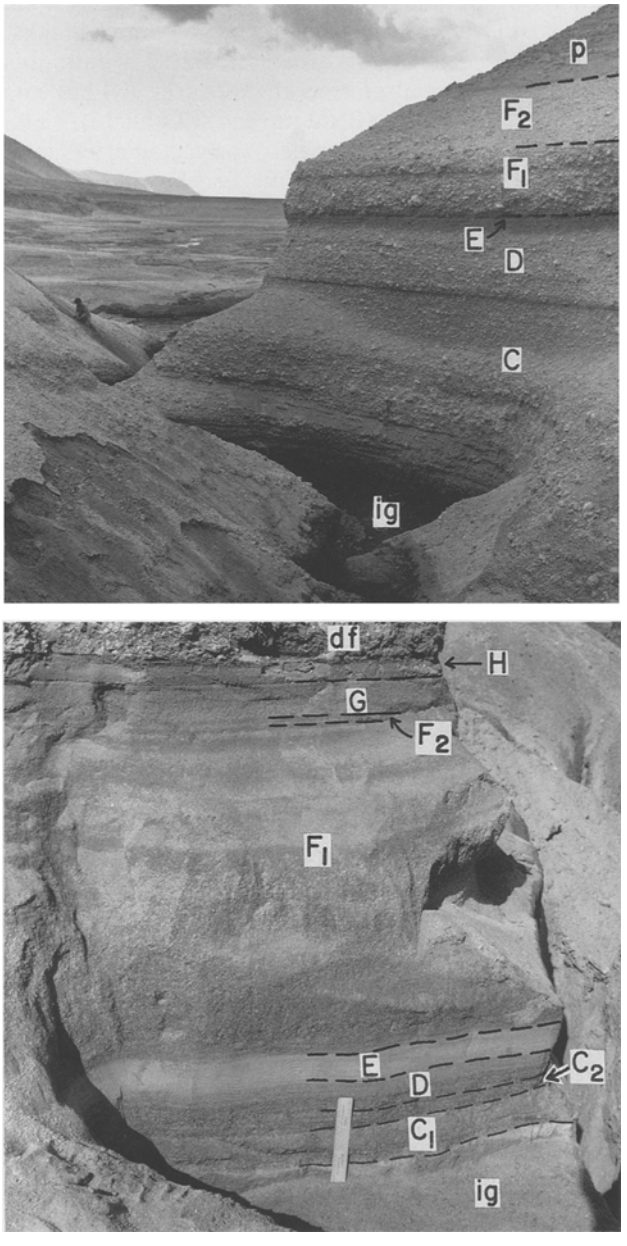

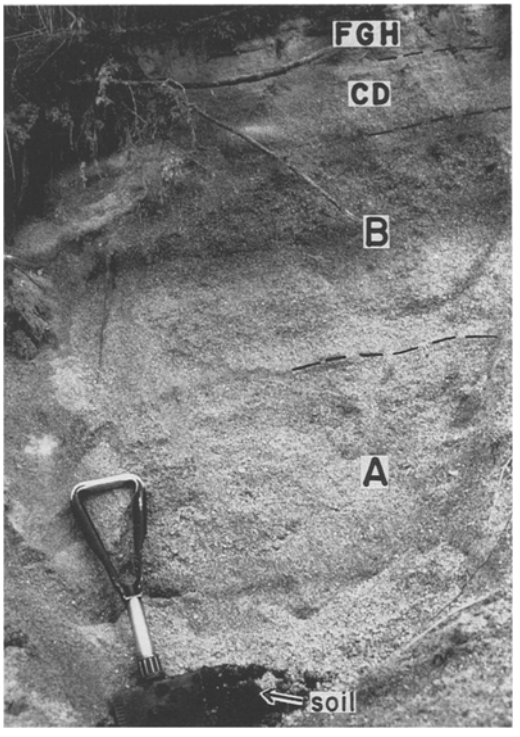

Fig. 13a–c. Fallout sections at different distances and directions from source (also see 11b). Ignimbrite (*ig*), fall layers (*A–H*), debris flow (*df*), and phreatic explosion deposits (*p*) are marked. **a** Knife Creek (section 2), 3.8 km, 040° from dome; Layer C rests here on 70 cm of fluvially reworked tephra (probably related to sheetflooding during break between flow and fall). **b** Lethe Hills margin of the VTTS (LH on Fig. 1), 12 km, 320° from dome; ruler is 15 cm long. **c** Geographic Harbor (section 8) 36 km, 120° from dome. Shovel is 58 cm long

such normal grading toward finer-grained (ash and granule) tops is well developed within the repeatedly interrupted post-ignimbrite sequence of plinian lapilli falls (Layers C–G) of Episodes II and III.

We conclude that virtually the entire ignimbrite sequence in the VTTS – excluding only the final andesite-rich flow units (and minor intraplinian flows emplaced during Episodes II and III) – was emplaced contemporaneous with accumulation of the Layer A–B plinian fallout. The volumetric rate of ignimbrite production increased as the erupting proportion of non-rhyolitic juvenile ejecta increased, and the mass ratio of plinian fallout to ignimbrite progressively decreased throughout the A–B succession (volumes and mass eruption rates are discussed below). The high-altitude plinian column fluctuated in intensity but nonetheless persisted through nearly all of Episode I, coexisting with ignimbrite generation for an interval of at least 11 h and perhaps as long as 16 h.

Eruptive Episodes II and III

Dacite fallout layers C–H

Several dacitic fall units that Curtis (1968) designated Layers C through H (Figs. 13–15) overlie either Layer B, the main VFI, or the heterogeneous HEPI. Layers C, D, F, and G are of plinian origin, and Layers E and H consist of fine ash that settled slowly at the ends of Episodes II and III, respectively.

Layer C is the coarsest and generally thickest of the post-ignimbrite plinian falls, and, in contrast to the rest of these (otherwise almost exclusively dacitic) fall units, its lowermost one-third contains up to 20% rhyolitic pumice (Table 2). As with Layers A and B before it, regional isopachs (Fig. 14) for Layer C demonstrate strong SE dispersal. The thickest known section of C is 6.2 m (~ 1 km W of Novarupta; Fig. 12, section 14) but closer to the vent its base is not exposed; 10 km downwind (SE) it is still 1.8 m thick. Layer C rests on fall Layer B_3 wherever the latter is present, but it lies directly atop the main VFI in the VTTS – where the final few ash flows were coeval with and later than B_3. Excluding the circum-vent ejecta ring, the basal part of Layer C has the coarsest ejecta of any 1912 fall deposit, containing pumice clasts as big as 45 cm at basal exposures SE of Falling Mountain. Ignimbrite flow units, 1–2 m thick and unusually rich in very coarse dacitic pumice blocks, occur directly beneath or are intercalated within this coarse fallout interval at several exposures 1–4 km east and west of Novarupta (BRU in Figs. 12 and 15).

Although Layer C is a single poorly graded fall unit near source and in upper Knife Creek where Curtis (1968) first described it, it is separable into two normally

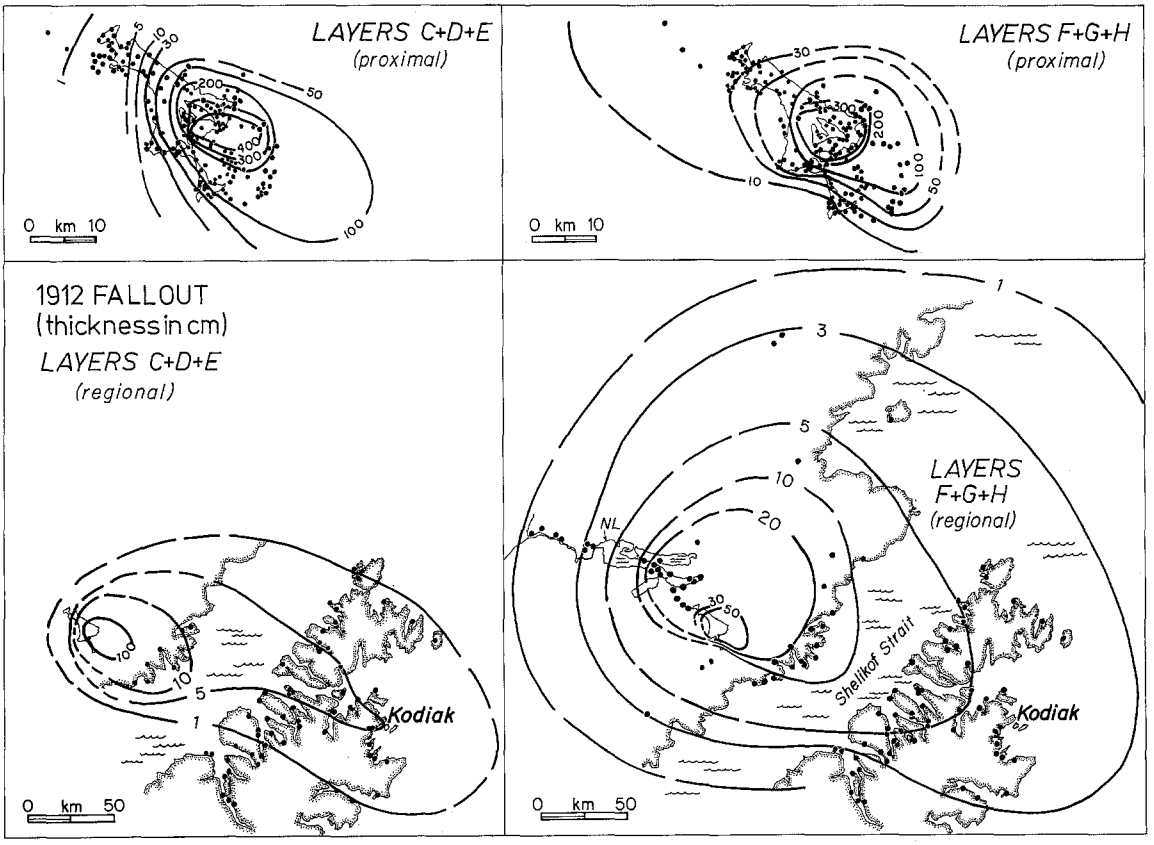

Fig. 14. Isopachs (in cm) of plinian Layers C + D and F + G. Because Layers E and H are discrete layers only in and near the VTTS, merging distally with CD and FG, they are here included in the CD and FG isopachs. Panels show proximal and regional distribution for each layer; VTTS ash flow sheet is outlined in each panel; Naknek Lake (*NL*) is outlined in FGH panel; shorelines as in Fig. 2

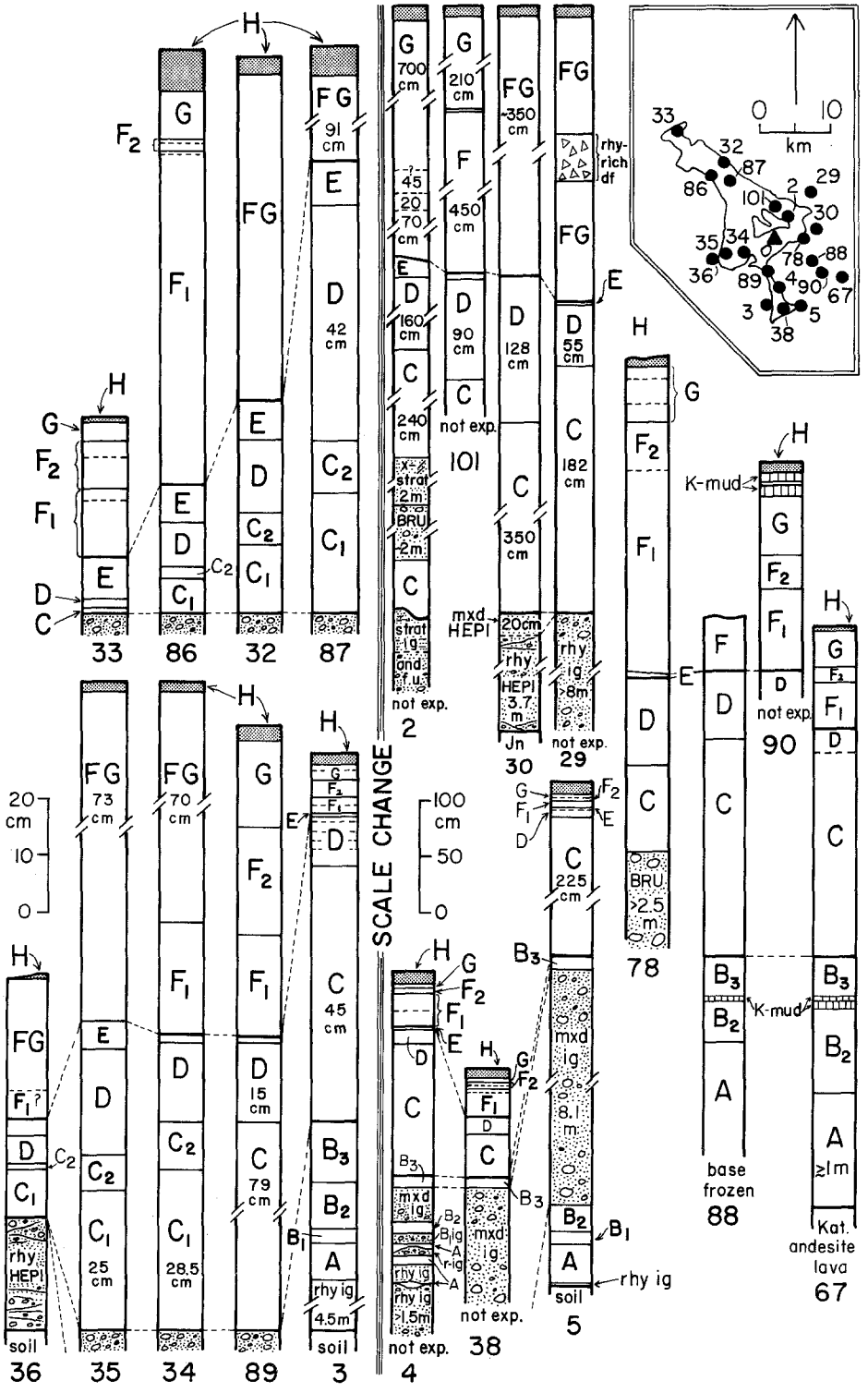

Fig. 15. Stratigraphic sections in and near the VTTS, located relative to the vent (*triangle*) and ignimbrite (outlined) in inset. Abbreviations as in Figs. 3 and 11. Ignimbrites (*patterned*) are compositionally heterogeneous (*mxd ig*) unless otherwise labelled. Plinian A–B fallout is confined to SE quadrant. Thickness of C–D fallout exceeds that of F–G in south; vice-versa to NW (cf. Fig. 14). *K-mud* in sections to SE are layers of nonjuvenile lithic ash expelled during caldera collapse of Mount Katmai. Rhyolite-rich pumiceous debris flows (*rhy-rich df*) consist of early ignimbrite remobilized (by snowmelt?) from slopes of Mount Griggs. Section 67 rests on Katmai andesite lava (*Kat. andesite lava*)

graded subunits (C_1 and C_2; Fig. 15) in and near the VTTS 8–19 km NW (upwind) of Novarupta. In the downwind direction (Fig. 14) south of Trident and Mount Katmai, Layer C is by far the thickest and coarsest unit of the dacite fallout sequence, consisting of only a single pumice-fall unit that is poorly graded except in the uppermost ~10% of its thickness, where it fines rapidly to crystal-rich ash and pumice granules. A normally graded top is well developed only at distances >7 km from vent, but in the proximal region a crystal-rich sandy parting 1–5 cm thick separates coarse, poorly graded, pumice-fall units C and D. The C–D parting appears to be time-correlative with a complex 2-m-thick flow/fall sequence intercalated with the plinian fallout ~1.5 km NW of source, on the vent-facing side of Baked Mountain (Fig. 12; section 1). Ash flows within that sequence were small, limited to a northwesterly sector, and their deposits thin away to only ~24 cm on the

SSW spur of Baked Mountain. The evident attenuation or remission in plinian activity between C and D must have been brief (and perhaps never complete), because there is no evidence for wind-reworking at this horizon, and because the parting is not fines-rich like Layer E, which settled during the longer suspension of plinian activity between Episodes II and III.

The thickest exposure of Layer D (2.2 m) is ~1 km W of Novarupta (Fig. 12; section 14) where it is a coarse non-graded dacitic plinian fall unit. In upper Knife Creek, where Curtis (1968) first defined Layer D, the upper 5–10% is normally graded, fining upward into dustfall Layer E, which marks the end of Episode II. Owing to the crystal-rich C–D parting just mentioned, Layers C and D are discrete throughout the VTTS. On the southern flanks of Trident and Mount Katmai where the parting is absent, Layer D rests conformably on the normally graded, crystal-rich top of C. Sandwiched between the much thicker and coarser lapilli falls C and F, Layer D thins downwind from 58 cm in the Trident saddles to ~20 cm at Katmai River. South of Trident and Katmai, it is everywhere normally graded, containing scattered 2-to-5-cm lapilli at its base but only crystal-rich ash and pumice granules at its top (Fig. 3; section 6 and 7). As no fine ash settled at the top of Layer C, it appears that Layer D is not the product of a wholly separate eruption but represents a late reinvigoration during waning stages of the fallout interval that produced Layer C. The slight coarsening that indicates the base of D downwind fades away with distance, and by Geographic Harbor 36 km from source (Fig. 3; section 8), Layers C and D are no longer distinguishable.

Episode III produced dacite falls designated Layers F and G in upper Knife Creek by Curtis (1968). In contrast to Episodes I and II, this fallout was not as strongly directed toward the SE, and regional isopachs (Fig. 14) for Layers FGH show slightly asymmetrical accumulation toward the NE. As F, G, and H are not separable >40 km from vent, much of this asymmetry may be attributable to northeasterly drift of slow-settling fine (coplinian) ash during the days or weeks after the plinian eruptions ended.

Layer F is proximally a complexly graded dacite pumice fall 3–6 m thick in upper Knife Creek, its basal 30–40% almost everywhere being markedly coarser than the rest (Fig. 13a), with pumice up to 30 cm common in the bottom half of the deposit out to ~3 km east of vent. Ultraproximally, in a limited NE to NW sector within 1.5 km of vent, the upper part of F also includes a distinct coarse interval having pumice blocks as large as 90 cm (Fig. 12; section 73). Medially, Layer F can be divided into two normally graded subunits (F_1 and F_2; Fig. 15), in the VTTS 10–21 km NW (upwind) of Novarupta as well as toward the SE on the flanks of Trident and Katmai. The subunits are weakly graded from lapilli and coarse ash to medium ash, with little or no fine ash at the top. As discussed earlier for Layers C and D, interruptions during or after deposition of plinian Layer F were brief and/or incomplete.

Throughout most of the VTTS and on the flanks of Trident and Mount Katmai, Layer G overlies F as a distinct weakly to non-graded fall capped by dustfall Layer H (Fig. 15). Locally in upper Knife Creek, Layer G is vaguely tripartite, having a basal non-graded and two poorly graded intervals. The several subunits of F and G were deposited in rapid enough succession that the grading was generally poor and fine-ash accumulation virtually lacking. The 1–2 cm fines-rich parting in upper Knife Creek where Curtis (1968) first defined Layers F and G is a local feature, probably representing material elutriated from small intraplinian ignimbrites intercalated with the F–G plinian deposits near Novarupta (Fig. 12; sections 14 and 109). The unity of the coarse F–G sequence in proximal locations and the fading distinction between Layers F_1, F_2, and G with distance from source (Fig. 3; sections 4–9) show that, as with Layers C and D, the F–G subunits do not represent significant time breaks in plinian activity. Many of the internal fluctuations within C–D and F–G are sectorially variable and probably reflect atmospheric turbulence and wind shear rather than syneruptive changes in vent configuration or column height.

Regional isopachs (Figs. 5 and 14) show strong SE-directed dispersal for Episode I and II ejecta but weaker NE and SE dispersal for Episode III. Curtis (1968) suggested that the three ashfalls reported at Kodiak (Martin 1913) correlated only with Episodes I and II and that none of the later FG fallout extended so far SE. Systematic thinning of the fall units (Fig. 3), clast composition proportions (Table 2), and the color zonation of distal ash layers (Fig. 3), however, combined with microprobe analyses of glass shards (Table 3), show that the final dacite plinian episode (FG) was nearly as voluminous as CD and, although not as strongly SE-directed as AB and CD, it did reach Kodiak village (Fig. 14; Table 3). The topmost layer on Kodiak Island, now 2–3 cm thick on the Shelikof coast (Fig. 3; section 9), is dacite-rich vitric ash (Table 3a) correlated with Layers FGH of Episode III.

On the basis of areally limited, proximal isopach data, Curtis also suggested that a change of wind direction had promoted NE-directed dispersal of Layer F and northerly dispersal of Layer G. The new (regional) data, however, show that the dispersal patterns for F and G (Figs. 14 and 15) may reflect not so much a change of wind direction as a relaxation of the earlier strongly SE-directed wind (Fig. 5), allowing somewhat more symmetrical distribution; this in turn could reflect in part the lower column height during Episode III (see below).

The dacite plinian deposits: componentry and sorting. In contrast to the 10–20% rhyolitic pumice in the basal part of Layer C (Table 2), dacitic Layers D–G (and most of C) contain only ~1% rhyolite (locally 3–5%) in proximal locations. Medially, however, the proportion of rhyolite pumice granules in D–G is larger (typically 6–12%) and locally as great as 16% in Layer F at Katmai River (Table 2). It seems likely that Layers D–G, which consist mostly of coarse ash and pumice granules at medial locations, contain a modest fraction of recycled (Episode I) rhyolite that was swept up into the column from near the vent. Except in the lower ~25% of

Layer C, the contributions of small rhyolite clasts to dacitic plinian Layers C–G are not thought to have actually *erupted* with the dacite, owing to (1) their scarcity in the coarser facies of these layers within ~6 km of vent; (2) their scarcity even medially (6–12 km) in most of Layer C (which is coarser than D–G); and (3) the extreme rarity of rhyolite-dacite banded pumice.

Accompanying the compositional change from Episode I to Episode II is a large increase in the free crystal content of the deposits. As individual dacite pumice clasts contain 30–45 wt% crystals (versus 1–3 wt% in the rhyolite), the Episode II deposits contain up to 67 wt% crystals at the N margin of the VTTS and still have 22 wt% crystals as far away as Kodiak Island (Table 4). Owing to the polycomponent nature of the ejecta, density sorting is superimposed on the general fining-with-distance trend of the fallout and, like thickness distribution, it varies sectorially around the vent and is greatly affected by wind. Each fall deposit has an annular crystal-enrichment zone in which the free crystal content of the deposit exceeds that in pumice clasts. A crystal-enrichment zone for Layer C, elongate due to strong winds, extends to the Ukak River ~20 km NE (67 wt% crystals) and at least as far SE as Shelikof Strait (~40 km; 45–49 wt% crystals). Available data indicate that the pattern for Layer F is similar, though the zone is probably smaller and somewhat less elongate (55 wt% crystals in upper Knife Creek; 56 wt% at the Shelikof coast).

Only a small fraction of the dacite fallout consists of lithic clasts, and the lithic-rich zones for the dacite falls are more restricted (i.e., within ~8 km of source) than are the crystal enrichment zones. There are generally fewer lithics proximally in Layer F (1–5 wt%) than in C (2–7 wt%; Table 4). Maximum lithic (ML) measurements confirm the more symmetrical distribution of Episode III ejecta vis-à-vis the strong southeasterly dispersal of Episode II ejecta (Fig. 16). Because Layers C and F are consistently coarser than D and G (respectively), their lithic isopleths are used to illustrate ML for Episodes II and III in Fig. 16. The fact that Layer F shows more restricted dispersal of lithics than either Layers A or C (Fig. 16) confirms that the third (FG) eruptive episode was the least vigorous.

Samples of the dacite plinian layers show a remarkably wide range of sorting ($\sigma_\phi = 0.7$–3.5), but those with high sorting coefficients (2.0–3.5) are all within 9 km of vent (Fig. 6). The poor sorting is in large part a result of the high crystal content of the dacite. Sieve analyses from various locations of the coarsest subunit within CD (C_1 in every case) and within FG (F_1) are shown in Fig. 7, all yielding cumulative frequency curves of similar shape. Ultra-coarse proximal deposits (<4 km from vent) have not been sieved. Layer C is always coarser than the other dacite layers at given distances SE of vent, even as far as Kodiak Island (e.g., for Layer C, Md = 1.55 mm at Katmai River, 0.47 mm at Geographic Harbor, and 0.09 mm on Kodiak Island versus 1.20,

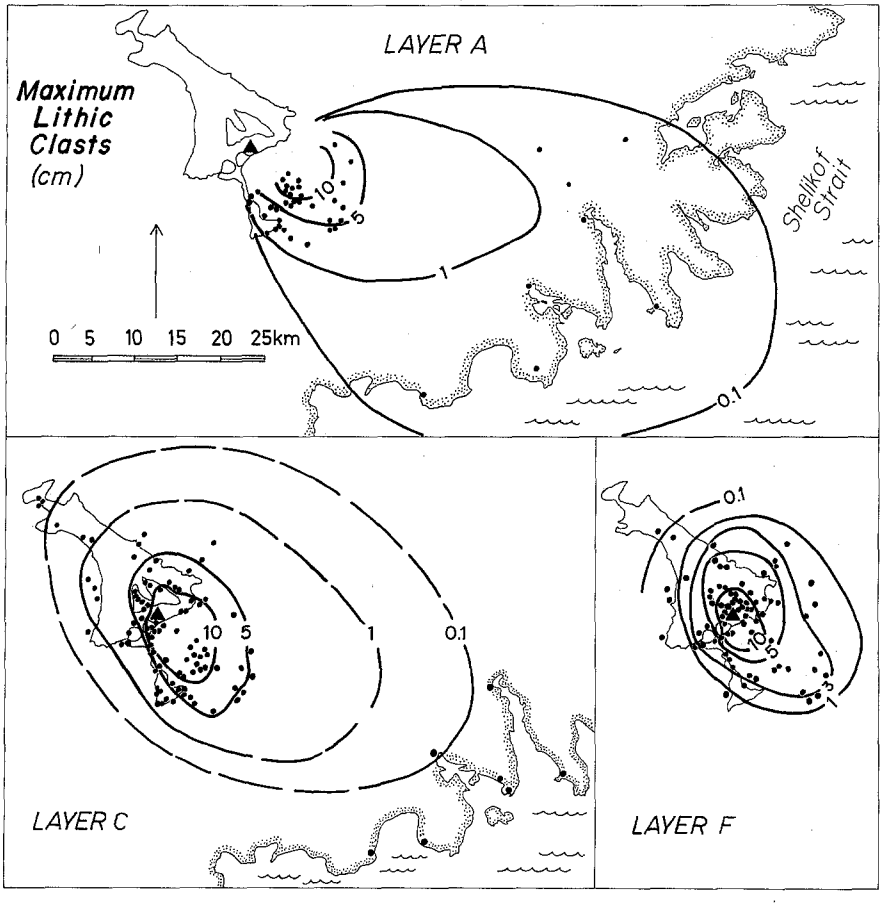

Fig. 16. Isopleths for average maximum lithic (*ML*) fragments in Layers A, C and F; C always has coarser lithics than D, and F than G. ML is the average length of three axes of 3–5 largest clasts at each site. VTTS is outlined and Novarupta is the *filled triangle*; *dots* are measurement locations. Scale is the same in each panel

0.26, and 0.06 mm, respectively, in Layer F). Rates of change in Md and σ_ϕ differ among fall units, especially toward the NW where median grainsize in Layer C decreases much more steeply than that of Layer F; e.g., over the 3.5 km between upper Knife Creek and the central VTTS, Md drops from 2.36 to 0.80 mm in Layer C but only from 1.18 to 0.59 mm in Layer F. Similarly, σ_ϕ changes rapidly in Layer C (from 3.41 to 1.63) relative to Layer F (from 1.46 to 1.13) at the same locations. Sectorial differences in the dispersal patterns of the several Episode II and III layers are thus evident in grainsize and sorting data as well as in isopachs and componentry.

Layer E

Layer E is a largely vitric dustfall of composite origin that settled during a break in the plinian eruptive sequence. It forms a continuous fine-grained rib between the CD and FG pumice-fall deposits for at least 23 km NW of the vent, as well as in Mageik Creek and in the saddles between the peaks of Trident. Farther toward the Pacific, Layer E is not definable as a separate unit, although equivalent dust may contribute to the normally graded top of Layer D near Katmai River.

In and near the VTTS, Layer E differs from the other fall deposits in having a relatively constant thickness of 5–9 cm and in having ≥ 50 wt% of the deposit finer than $+4_\phi$ (63 μm). Only at near-vent locations is it coarser (Md up to ~0.5 mm), there having as little as 11 wt% finer than 63 μm (Fig. 7). Component analyses of Layer E show a range of 9–19 wt% crystals (mostly <0.25 mm; with almost no quartz) and very few lithics; samples having >10 wt% crystals are all from the upper VTTS (Table 4). For example, in Upper Knife Creek (4 km from source) Layer E has 13 wt% crystals and 0.5 wt% lithics, but at 23 km NW of source it has 9 wt% crystals and virtually no lithics.

Near-vent flow deposits exposed at the stratigraphic position of Layer E include: (1) lenticular surge layers on Broken Mountain 2.8 km N of Novarupta (Fig. 12; section 27); and (2) thin (<2 m) intraplinian ignimbrites exposed in gulches 1 km N of Novarupta dome, immediately S of Falling Mountain as far as 2 km SSW of the dome, and in the major gulch system 2 km ENE of the dome (Fig. 12; section 19, 20, 21, 73 and 109). These deposits contain subordinate andesitic and rhyolitic pumice but, like Layer E, they are dominantly dacitic; their accompanying ashclouds certainly contributed to Layer E fallout proximally, but its relatively constant thickness suggests a widespread lingering dustcloud as the source for much of Layer E in medial to distal parts of the VTTS and adjacent valleys.

Microprobe analyses show that Layer E ash is mostly dacitic, 86–95% of its glass shards being derived from dacite pumice (Table 3). Although its distribution and large fraction of fine ash seem to suggest some relation to the VTTS ignimbrite, Layer E is not predominantly a co-ignimbrite ash deposit (cf. Sparks and Walker 1977). The microprobe data (Table 3) yield averages of ~6% rhyolitic and 94% dacitic and andesitic shards in Layer E. As ~2/3 of the ignimbrite consists of rhyolite and ~1/3 of dacite and andesite, if we assume that *all* of the rhyolitic shards in Layer E are ignimbrite-derived, then the maximum co-ignimbrite ash contribution to Layer E is 9% (6% rhyolitic and 3% dacitic and andesitic ash). Nonetheless, Layer E does contain a few percent whole-bubble shards unique to the rhyolitic ejecta of Episode I. Unlikely to have been recycled from (generally welded) vent-filling material, these delicate spheres must have been erupted during Episode I and held aloft turbulently until this post-Episode-II hiatus. Glass shards in Layer E therefore clearly have a composite origin: most were erupted with dacitic Layers C and D, a small fraction is co-ignimbrite or co-plinian fine ash from Episode I, and in the upper VTTS a significant local contribution was added by ash clouds generated by small proximal pyroclastic flows during Episode II.

Layer H

Wherever preserved in or near the VTTS, Layer H stands out as a 5–50-cm-thick mud layer capping the 1912 primary deposits. It consists predominantly of fine vitric ash and, even proximally, >50 wt% is finer than 63 μm (Fig. 7); its crystal content is generally ≤ 10 wt% and its lithic fraction is negligible (except on Mount Katmai). Layer H locally contains visible accretionary lapilli, and in places it has a vesicular structure that may reflect syndepositional incorporation of atmospheric moisture and perhaps partial homogenization of accretionary-lapilli-rich fallout (Rosi 1992). As Layer H merges distally with the fine top of Layer G, it is not separately definable >20 km NW nor >40 km SE of Novarupta.

Microprobe analyses (Table 3) show that in most places near the VTTS 85–100% of the glass shards in Layer H were derived from the dacitic juvenile component; only in a few locations marginal to the ignimbrite have rhyolitic and andesitic glass been found to exceed 10% of the total shards present. On the slopes of Mount Katmai, however, lithic dust generated during caldera collapse is intimately mixed into Layer H (Hildreth 1991). Rhyolitic shards are far more abundant downwind, making up 23–40% of the uppermost few centimeters of ash SE of Shelikof Strait (Table 3); to the northwest, on the other hand, the rhyolitic shard fraction in the uppermost ash drops off from 19% at Brooks Camp (50 km NW) to only ~1% at King Salmon (100 km NW).

Most rhyolitic shards within Layer H in and near the VTTS were probably elutriated from the ignimbrite, because most fine ash in the rhyolitic plinian column rose to great elevations and was strongly blown toward the SE (Fig. 5). If we assume that near the VTTS Layer H contains an average of 6% rhyolite (Table 3a), that none of this rhyolite is from plinian phases A and B, and that the ignimbrite is 2/3 rhyolite and 1/3 dacite and andesite, then just as for Layer E the maximum co-ignimbrite contribution to proximal-medial Layer H is ~9%

(6% rhyolite, 3% intermediate). The rest is mostly fine dacitic ash that settled slowly after the dacitic plinian eruptions of Episodes II and III. Because Layer H is not appreciably coarser or thicker near Novarupta than in the Knife Creek and River Lethe arms of the upper VTTS, and since no consistent internal stratigraphy is recognized within this (largely massive) dustfall unit, it seems unlikely that any minor eruptive activity continuing after Episode III (or during dome emplacement) contributed significantly. The process by which more rhyolitic shards were incorporated into the topmost distal ash downwind than into proximal-medial Layer H is addressed below (see *Co-plinian versus co-ignimbrite ash*).

Intraplinian fall and flow deposits

Associated with the plinian layers of Episodes II and III but restricted to the proximal region within ~4 km of Novarupta are numerous thin ignimbrites and scoria-rich fall units. Although >99% of the ejecta were distributed as plinian fallout, small proximal intraplinian ignimbrites were repeatedly generated throughout these episodes.

Block-rich pyroclastic flow deposits 0.5–2 m thick, dominated by dacitic (and fewer andesitic) pumice clasts as coarse as 20–50 cm, directly underlie Layer C or are intercalated within its coarse basal part. These block-rich units (BRU in Fig. 12) crop out along the floors of several gulches east and west of Novarupta, and in upper Knife Creek another (locally water-remobilized along the stream channel) is underlain by 40 cm of Layer C plinian fallout (Fig. 15; section 2). The unusually coarse pumice in these flow units is comparable to that in proximal exposures of the base of Layer C near Falling Mountain (Fig. 12). The block-rich units are thought to have been generated during a brief 'throat-clearing' period of low fountaining leading up to re-establishment of the plinian column at the opening of Episode II.

Exposed within the Layer C fallout on the southern spurs of Baked Mountain (Fig. 1) is a thin (1–20 cm), matrix-rich, oxidized flow or surge (Fig. 3; section 1). This flow pinches and swells on a decimeter scale and thins to an obscure sandy parting on the SSW spur, 2.3 km from source.

Overlying Layer C on the southern spurs of Baked Mountain is a 2-m-thick, lenticularly stratified, composite flow-fall sequence that contains 25-to-50-cm ballistic blocks of dense vitrophyre, angular fallout pumice clasts, and flow-rounded pumice clasts (Figs. 3 and 12; section 1). On the opposite (south) side of the vent is a similar 2.5-m-thick, but somewhat finer-grained, sequence of alternating lapilli-rich and sandy layers that appears to be at the same stratigraphic horizon (Fig. 12, section 110). These poorly sorted andesite-bearing, lithic-rich flow-fall deposits extend only 1–3 km from vent. They apparently correlate with the widespread C–D sandy parting and represent only a brief change in vent conditions, involving an influx of andesitic magma and a vent-wall spalling event that promoted transient disruption of the plinian dacitic eruption.

Small proximal pyroclastic-flow deposits sandwiched between plinian Layers D and F (Fig. 12) have already been mentioned in the discussion of Layer E.

Intercalated proximally with the upper dacite fall deposits (Layers F and G) are (1) a few coarse andesite-bearing fallout layers (one as thick as 4 m) that are well-exposed in the ejecta ring around Novarupta but pinch out within 1 km of source; (2) two small intraplinian ignimbrites, 1–3 m thick, which extend as far as 2.3 km west and 2 km east of the dome (Fig. 12; sections 14 and 109); and (3) several thin (10–25 cm) lenticular flow or surge sequences exposed in the ejecta ring and in big gulches 1 km south of Novarupta (Fig. 12; section 110). Although andesite-bearing, the fallout deposits are predominantly dacitic, and the andesite component decreases rapidly away from the vent. Pumice counts proximally and medially (Table 2) and microprobe work on glass shards downwind (Table 3) show that andesite scoria was mostly restricted to pyroclastic flows and to low fountains depositing near vent and was never introduced as more than a minor component into the plinian columns.

Discussion

Lithics and the 1912 vents

Maximum lithic (ML) clast distributions (Fig. 16) show that downwind axial dispersal progressively decreased from Episode I through II to III. ML plotted against total lithic dispersal area (Fig. 17), however, shows that Layer C lithics are more widespread than those of Layer A. Although plinian Layer A was more voluminous (Table 5), farther-travelled (Figs. 5 and 14), and by many criteria was more energetic than all subsequent plinian phases, its narrow unidirectional dispersal sector (Fig. 5) makes it appear less widely dispersed than Layer C in Fig. 17. Fallout thickness plotted against isopach area, however, clearly shows that Layer A was more widely dispersed than Layers C and D combined (Fig. 18). Lithic dispersal patterns alone, therefore, without consideration of isopach and isopleth shapes, may be inadequate as a standard of comparison among eruptions.

Of all the fall units, Layer A is by far the richest in lithic fragments, containing as much as 24 wt% lithics on the S flank of Trident and 12 wt% lithics even 40 km downwind (Table 4). At the same locations (along Shelikof Strait) the dacite plinian units have <1 wt% lithics, and even proximally they have only 1–7 wt%; moreover, most of these lithics are cognate vitrophyre rather than accidental wallrock fragments (Hildreth 1987). Similarly, the all-rhyolite HEPIs, containing 9–14 wt% lithics, are far more lithic-rich than their compositionally heterogeneous equivalents; although a few layers have 5–16 wt% lithics, most have <2 wt% (Table 4). The higher proportion of lithics in Phase A is presumably due to (1) initial opening and reaming of the vent and (2) the dacite vent being nested within vent-filling fallback tephra

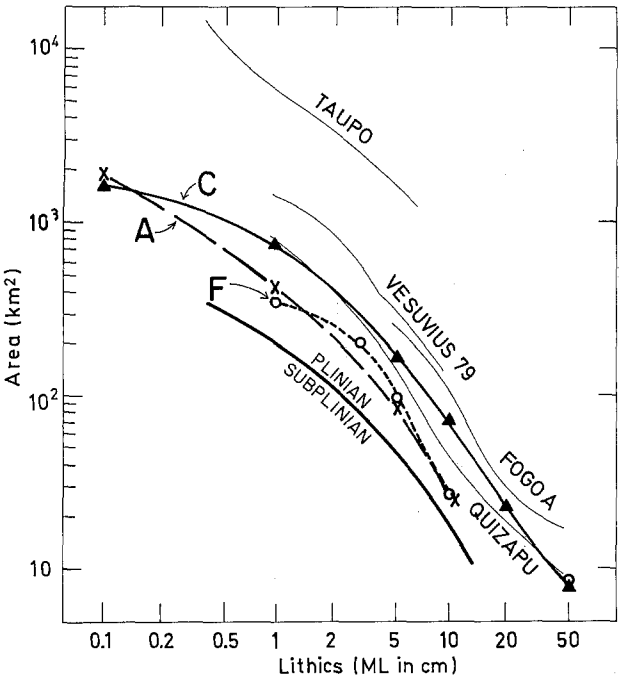

Fig. 17. Area in km^2 enclosed by isopleths of average maximum lithic clasts (*ML*) for Layers A, C, and F. Plinian and subplinian fields (defined by Walker 1981) are labelled. Quizapu 1932 (Hildreth and Drake 1992), Taupo plinian (Walker 1980), 79 AD Vesuvius (Sigurdsson et al. 1985), and Fogo A (Walker and Croasdale 1971) are included for reference

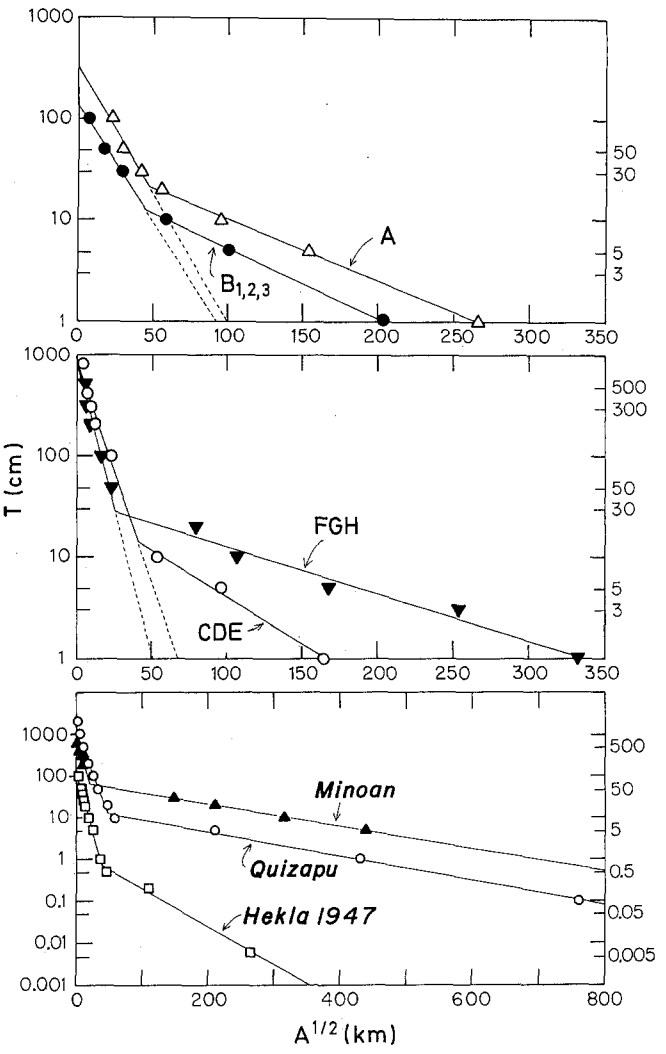

Fig. 18. Plot of thickness (log scale) versus area$^{1/2}$ (after Pyle 1989). Straight-line segments define exponential thinning; break-in-slope in each line is thought to represent the 'decoupling limit', beyond which the accumulated ash is largely 'co-plinian'. Distally, FGH appears most voluminous because it includes co-plinian ash from AB and CDE. Volumes were calculated (Table 5) by integrating under each segment separately, following Fierstein and Nathenson (1992); *Dashed lines* are projections of simple exponential thinning, as discussed in text. Also illustrated are data for three other deposits that show such two-segment thinning: Hekla 1947 (Thorarinsson 1954), Minoan eruption of Santorini (Pyle 1990), Quizapu 1932 (Hildreth and Drake 1992); note the scale change

rather than breaking through brittle wall rocks, as had the rhyolite a day or so earlier. All of the Episode II and III ejecta erupted from a nested inner vent <400 m wide, which the Novarupta dome now plugs, and they heavily mantle the 2-km-wide structural depression that had been the larger source area of the main pyroclastic flows (Hildreth 1987). Although nowhere exposed, the Episode I vent system is thought to have enlarged and evolved complexly, as indicated by (1) the size and structure of the Novarupta depression (Hildreth 1983, 1987; Wallmann et al. 1990); (2) the distribution of compositionally varied HEPIs on scarp rims surrounding the depression; and (3) the changing proportions of lithic fragments of Naknek sedimentary rocks, Trident andesites, and Falling Mountain dacite in the sequence of Episode I deposits. Near-vent deposits and structure are under continuing investigation.

Distal ash and the fallout record at Kodiak

The three distinct periods of ashfall on 6–9 June 1912 at Kodiak village (Martin 1913; Griggs 1922) probably reflect the three main eruptive episodes. Our 58 measured sections on Kodiak, Afognak and Shuyak Islands, however, document as many as six color zones in these fine-grained distal fallout deposits (Figs. 3 and 7). The zones are generally gradational in grainsize but can usually be recognized and correlated from one location to another; the only relatively sharp contact is between the two uppermost zones. A representative section with all six zones (here called 1 to 6) well defined is given in Fig. 3 (section 9) from the area of thickest deposition in the main dispersal direction on Kodiak Island (Uganik Bay; Fig. 2).

Field correlations based on grainsize and color are supported by microprobe analyses of shards that show both the basal white, coarse-to-medium ash zone 1 (Md = 0.36 mm) and the overlying, slightly finer-grained light-pink ash zone 2 (Md = 0.29 mm) to be 100% rhyolite (Table 3). Accordingly, they are together equivalent to Layer A. Zone 2 grades upward to a thin zone of dark salmon, medium ash (zone 3, Md = 0.29 mm) and a zone of lighter-salmon fine ash (zone 4, Md = 0.13 mm)

Table 5. 1912 fallout volumes

a Accumulated volumes and adjusted volumes erupted
Calculation method: log T vs $A^{1/2}$ graph + integration (Fierstein and Nathenson 1992, modified after Pyle 1989)

Eruptive unit	Volume to interception point[a]	Volume beyond interception point[a]	Total (volume accumulated)	Strictly plinian[b]	Co-plinian + co-ignimbrite	Compositonal[a] adjustment		Total volume erupted (Adjusted)	DRE[d]
						Rhyolite	Dacite		
A	1.50	3.60	5.10	1.97	3.13	+1.05	—	6.15	2.10
$B_1+B_2+B_3$	0.68	1.65	2.33	0.81	1.51	+0.35	—	2.67	1.02
CD+E[c]	1.51	1.19	2.70	1.65	1.05	−0.41	+2.47	4.76	1.99
FG+H[c]	0.82	6.23	7.05	0.97	6.08	−1.14	−2.47	3.44	1.66
								17.02	6.77

Accumulated volumes within dispersal sectors[e]

Eruptive unit	NE	SE	SW	NW	Sub-total
A	0.07	4.95	0.08	0	5.10
$B_1+B_2+B_3$	0.06	2.20	0.04	0.03	2.33
CD+E[c]	0.53	1.72	0.33	0.12	2.70
FG+H[c]	3.30	1.70	0.54	1.50	7.05

b Tephra volumes calculated by other methods[f]

Eruptive unit	(1)	(2)	(3)	(4)
	to 1 cm	to 1 cm	to infinity	to 0.1 cm
A	6.4	7.2	6.3	—
$B_1+B_2+B_3$	2.4	2.6	4.9	—
CD+E[c]	3.4	3.8	5.7	2.6
FG+H[c]	7.2	7.7	10.9	—
Total	19.4	21.3	27.8	2.6 (CDE only)

(1) Thickness-area graph to 1 cm using the trapezoidal rule
(2) Thickness-area graph to 1 cm using a modified trapezoidal rule (after Froggatt (1982))
(3) Thickness-area graph using a two-straight-line approximation and extrapolating to infinity (after Rose 1973)
(4) Mass balance calculations using crystal/vitric ratio (35/65) (after Walker 1980)

[a] The volume beyond the break in slope (interception point) on a log T vs $A^{1/2}$ plot is used to calculate the amount of co-plinian CD that is included in Layer FG (see Fig. 18). Sector volume calculations permit redistribution of rhyolitic co-plinian ash into correct units. The total rhyolitic ash included in the dacitic falls is ~1.55 km^3; assume 10% is co-ignimbrite (0.155 km^3), then 1.4 km^3 is co-plinian. Considering clast proportions in Layers A and B, 75% of the co-plinian rhyolite (1.05 km^3) is assigned to Layer A and 25% (0.35 km^3) to Layer B

[b] 'Strictly plinian' is the exponential thinning distribution represented by a single straight line (dashed lines in Fig. 18)

[c] Layer E is only distinguishable in and near the VTTS, merging with C-D more distally; Layer H is a separate layer as far 15 km from vent but merges with F-G more distally.

[d] See Appendix 1 for conversion of tephra volumes to dense rock equivalents (DRE, magma volumes)

[e] For calculation purposes, azimuths chosen as midlines for sectors were ~45°, ~110°, ~190°, and ~300°

[f] These methods are compared in Fierstein and Nathenson (1992); we consider the log thickness vs area$^{1/2}$ graph to be the best method now available

that have 90% and 77% rhyolitic shards, respectively, nearly all other shards being dacitic. Although these zones are markedly different in color from underlying zones 1 and 2 – which is probably what led Martin (1913) to correlate them with the second period of ashfall – these are considered part of Episode I and correlative with Layer B, but they certainly include contributions of slow-settling shards erupted during Phase A of Episode I. The overlying tan fine ash (zone 5, Md = 0.09 mm) has 37% rhyolitic shards, and the capping light-grey fine ash (zone 6, Md = 0.06 mm) has only 29%; as both are dominantly dacitic, they are correlated with Layers CD and FGH, respectively. The exact rhyolite-to-dacite proportion varies somewhat from one place to another on both sides of Shelikof Strait (Table 3), but the fraction of rhyolitic shards always decreases upward from zone 1 to 6.

In contrast to this systematic stratigraphy in the downwind sector SE of Shelikof Strait, distal fallout is generally unstratified in off-axis sectors. For example, visually homogeneous single layers of fine ash are ~28 cm thick on the south shore of Naknek Lake (~32 km NW of Novarupta), 2 cm thick near King Salmon (100 km NW), and 4 cm thick on Augustine Island (160 km NE). At all such distal off-axis sections studied, the fallout consists mostly of vitric ash derived from dacite pumice (Table 3). Although rhyolite-derived shards are also present (1–19%; Table 3a), rhyolite-*dominated* distal fallout is confined to the downwind (SE) sector; in other directions, most of the slow-settling fine ash was ejected in the dacitic plinian events of Episodes II and III.

Co-plinian and co-ignimbrite ash

Although the downwind stratigraphic fallout sequence on Kodiak Island is generally similar to those at Mageik Creek, Katmai River, and along the mainland side of Shelikof Strait (Fig. 3; section 5–9), it is complicated there (and to a lesser extent at other distal locations) by extended deposition of fine rhyolitic ash (also see discussion of Layer H). Incorporation of 25–40% rhyolitic shards into the near-axis distal fallout (Table 3) from the predominantly dacitic eruptions of Episodes II and III shows (1) that the uppermost distal ash zones are a composite product of rhyolite-rich Episode I and the later dacite eruptions; and (2) that a large mass of the lower-density rhyolitic ash had remained aloft throughout Episodes II and III. Although some fraction of these rhyolitic shards may have been swept up and recycled from previously erupted rhyolitic ejecta in and near the vent area, it is probably a limited contribution, because rhyolite clasts comprise only ~1% of proximal CD and FG fallout (within ~6 km of source), because the vent for the dacite eruptions was no wider than 400 m, and because much of the vent-filling rhyolite was by then welded. Concurrent eruption of large volumes of rhyolite and dacite (and andesite) took place only during Phase B, ~80% of the products of which were emplaced as ignimbrite.

The post-plinian fine-grained fallout deposit (Layer H) capping proximal-medial sections from the VTTS to Katmai River contains only a small fraction (<10%) of co-ignimbrite ash, as discussed above, because of its limited content of rhyolitic shards (Table 3). The scarcity of co-ignimbrite ash in and near the VTTS may be attributable to (1) partial flushing by the dacite plinian falls; (2) the relatively low-energy emplacement of the ash flow sheet, promoting only modest elutriation of fines from the moving flows; and (3) the continuing influence during Phase B of a high eruption column, coexisting with ignimbrite generation and drawing some of the near-vent ash cloud up into the plinian column. The rhyolitic shards that make up 25–40% of the uppermost layers (color zones 5 and 6) on both sides of Shelikof Strait must therefore be leftovers from the Episode I plinian phase. Column height was greatest during Phase A, favoring preferential high-altitude retention of the lower-density rhyolitic shards that were sustained aloft by atmospheric turbulence throughout the subsequent eruptive episodes. On the other hand, because Episode I fallout was blown so strongly to the SE (Fig. 5), the minor fractions of rhyolitic shards (Table 3) in the uppermost ash to the NW and NE could well be mostly of co-ignimbrite origin.

Shards that settled distally into a given layer are thus not all from the same eruptive episode; each successive eruptive pulse flushed some of the fine ash held aloft between episodes. As the rhyolitic shards (mostly <125 μm) are dominantly plinian in origin, their settling behavior was evidently physically decoupled from the coarser co-eruptive plinian ejecta that fell as Layers A and B, and by analogy with the term co-ignimbrite, could be called 'co-plinian'.

It seems likely that the rhyolitic co-plinian ash suspended for hours or days after the eruption did not follow 'normal' trajectories as modeled by Wilson (1972) or Carey and Sparks (1986), but instead had fallout paths and settling velocities greatly affected by atmospheric turbulence. Wilson (1972) indeed suggested that turbulence can make it 'no longer appropriate to think of small particles as being launched from the vent with a specific velocity and elevation'. Plots of isopach data using log thickness versus area$^{1/2}$ coordinates (Pyle 1989) are expected to be straight lines because of the well-documented exponential thinning characteristic of many fallout deposits. Isopach data for the 1912 eruption and for three others so represented (Fig. 18) all yield straight, but two-segment, best-fit lines with a break-in-slope – beyond which area increases at a greater exponential rate – for medial-to-distal deposits well beyond the proximal area that could have been affected by surges, ballistic ejecta, or other near-vent phenomena. The medial to distal breaks-in-slope are seen as a 'decoupling limit' where ash that did not follow 'normal' fall trajectories becomes important or dominant and is fine enough to have been affected by different settling processes (e.g., ash clustering; Carey and Sigurdsson 1982; Schumacher 1990). The steep line segments represent coarser, proximal-to-medial ejecta that followed conventional fallout trajectories (Wilson 1972; Carey and Sparks 1986); the flatter segments represent distal tephra that includes some 'normal' plinian fallout as well as slow-settling fines that remained aloft longer (and were transported farther) than predicted by terminal fall velocities (cf. Walker et al. 1971; Wilson 1972; Wilson and Huang 1979).

We do not consider the decoupled fallout paths of fine distal ash 'abnormal'; to the contrary, we suggest that the independent dispersal of fine particles – although seldom documented or quantified in fallout distribution models – represent typical plinian behavior. Although the large fraction of fine ash (>50 wt% finer than 63 μm) in 1912 plinian deposits may have been enhanced somewhat by drawing back up into the convecting column part of the peripheral ashclouds generated by concurrent production of ash flows, this is not an essential contribution. The comparably voluminous 1932 rhyodacite eruption of Quizapu produced a plinian deposit having ~50 wt% of the ejecta finer than 63 μm (Hildreth and Drake 1992) and a similarly inflected thickness-area relationship (Fig. 18), even though ignimbrite generation was negligible.

Volume estimates

Isopachs for the 1912 fall layers (Figs. 5 and 14) are based on our 382 measured sections from Naknek to Kodiak (Figs. 1 and 2), on reports by Martin (1913) and Griggs (1922), and on a few seafloor core data from the Gulf of Alaska (Nayudu 1964; Federman and Scheidegger 1984). Although fall Layers A and B_{1-3} accumulated without significant interruption from the first plinian column, the A–B transition represents a fundamental

change in eruptive style, in that ~90 vol.% of Phase A was emplaced as fallout and ~80 vol.% of Phase B as ignimbrite. Layers A and B_{1-3} are therefore contoured on separate isopach maps (Fig. 5). The irregularly shaped 1912 isopachs (Figs. 5 and 14) are not well approximated by circular or elliptical mathematical expressions, so area determinations for each isopach out to 1 cm (Fig. 18) were made by planimeter and checked by counting km^2 boxes on a grid overlay.

Novarupta's collective fallout (Fig. 2) was previously estimated to have a tephra volume of ~20 km^3 (Griggs 1922; Curtis 1968; Hildreth 1983). Our new data now permit calculation of fallout volumes for each of the eruptive episodes: 8.8 km^3 for Episode I (6.1 km^3 for A; 2.7 km^3 for B_{1-3}); 4.8 km^3 for II; and 3.4 km^3 for III, yielding a total volume estimate of 17.0 km^3 (Table 5a). These estimates employed a modified version of Pyle's (1989) method, using integration to vanishing thickness, and showing that 9–14% of the volume of each of the fallout layers lies beyond the 1 cm isopach (Table 7; Fierstein and Nathenson 1992). Owing to the mixing of slow-settling fine ash from successive episodes, eruptive and depositional volumes are quite different, a problem that required several adjustments.

Because the proportion of rhyolitic ash is sectorially highly variable, fall-unit volumes calculated by the same method (Fierstein and Nathenson 1992) but *by sector* (Table 5) were combined with shard-composition proportions determined by microprobe (Table 3) to estimate the total amount of rhyolitic ash in each unit. On this basis, it is determined that a total of 1.55 km^3 of fine rhyolitic ash in the otherwise dacitic fallout Layers C through H (Episodes II and III) had actually erupted during Episode I; accordingly, the reapportionments made in recalculating the plinian *eruptive* volumes of each episode are outlined in Table 5.

At least 90% of the 1.55 km^3 of reapportioned rhyolitic ash is thought to be of co-plinian rather than co-ignimbrite origin, almost exclusively so in the distal downwind (SE) sector. As discussed above, <10% of the (predominantly dacitic) fine ash overlying or adjacent to the ignimbrite in the VTTS and Mageik Creek (Layers E and H) can be of co-ignimbrite origin. Even to the N and NW of the VTTS, where nearly all rhyolitic ash might be presumed to be co-ignimbrite, the proportion of rhyolite shards in the (unstratified) fine ash layer drops off from 7–19% medially (32–49 km from vent) to <1% distally (100 km NW) (Table 3).

An additional problem requiring volume adjustments is that beyond ~20 km from source Layers F, G, and H merge and become indistinguishable so that the distal FGH layer contains not only F–G ejecta but co-plinian C–D ash, co-plinian A–B ash, and (to the NW and NE) a little co-ignimbrite ash as well. To address this problem, the volume represented by each line segment in Fig. 18 was calculated separately for each eruptive unit (Table 5a), and then the volumes assumed to have had conventional fall trajectories – i.e. observing exponential thinning distributions represented by projecting single medial straight lines (dashed lines in Fig. 18; 'strictly plinian' in Table 5a) – were subtracted from the total volumes. We assume that the remainder is predominantly fine ash that represents the combined co-plinian and co-ignimbrite ash volume (with a minor contribution from recycled vent-filling ejecta). All rhyolitic co-plinian and co-ignimbrite ash in Layers C–H was reassigned to Episode I, and the dacitic fine ash beyond the break-in-slope for FGH was reapportioned evenly between Layers CD and FG. As summarized in Table 5a, about half of the 7.1 km^3 of Layer FGH can thus be shown to have erupted during preceding eruptive episodes.

Volumes by other methods. Tephra volumes calculated by a few other methods are summarized in Table 5b. Out to the 1-cm isopach, the trapezoidal rule – a numerical integration method for approximating the area under a curve – gives 19.4 km^3, and a modified trapezoidal rule (Froggatt 1982) gives 21.3 km^3. When integrated to zero thickness, a plot of area versus thickness (Rose et al. 1973) gives 27.8 km^3. Fierstein and Nathenson (1992) compare the mathematics of each of the above methods and agree with Pyle (1989) that integration of the log thickness versus $area^{1/2}$ plot provides the most rigorous and realistic method for calculating fallout volumes. An important consideration in the case of the complex 1912 fallout sequence is that deposit volumes given in Table 5b are not adjusted for the mixing of contributions from successive eruptive episodes. It may be a widespread problem for other complex eruptive sequences that such calculations only represent how much ash *accumulated* during the different stages of an eruption, not how much ash actually *erupted* during each phase (as elaborated in Table 5a).

The log thickness versus $area^{1/2}$ method provides a good estimate of the volume of a fall deposit if there are adequate isopach data (Fierstein and Nathenson 1992). Walker's (1980) crystal concentration method was developed to deal with the common case of poorly constrained distal isopachs. That method is quite sensitive, however, to the assumed crystal/glass ratio in pumice clasts, as discussed by Fierstein and Nathenson (1992). As an example, accepting Walker's (1980) deposit masses on-land, if the average crystal content of the pumice were changed from 3 wt% to 4% or 2%, then the total volume of the Taupo Plinian would change from 23 km^3 to 18.6 km^3 or 31.5 km^3, respectively (Table 6). Because of the wide range of crystal contents in 1912 pumice (and in many eruptive units), the crystal-concentration method is difficult to apply here. For example, if an *average* crystal content of 35 wt% for 1912 dacite is adopted, we calculate an accumulated volume of 2.6 km^3 for CD, (including 0.3 km^3 of 'lost' glass), similar to that obtained by other methods (Table 5). The crystal content of the dacite pumice is widely variable, however, and is as great as 45 wt%, which would result in a negative value for the 'lost' glass (Table 6).

Dense rock (magma) equivalents. At similar distances from source, bulk density of each fallout deposit varies sectorially around the vent, depending largely upon crystal contents and whether the glass component is mostly pumice lumps or tiny shards. As bulk densities

Table 6. Volumes using mass balance method

Taupo plinian[a]		
Crystal/glass	Tephra volume	
2:98	31.5 km^3	
3:97	23 km^3	
4:96	18.6 km^3	
5:95	16 km^3	
Novarupta 1912: plinian CD		
Crystal/glass	Tephra volume	'lost ash'
30:70	3.02 km^3	0.7 km^3
35:65	2.62 km^3	0.3 km^3
40:60	[b]	−0.03 km^3
45:55	[b]	−0.3 km^3

[a] Data for Taupo plinian from Walker (1980)
[b] Total volume is not estimated because calculations yielded a negative value for lost ash, implying that some assumption(s) in the calculations (crystal/glass ratio?) is incorrect

change both sectorially and with distance from source, a bulk deposit density for each of the three major plinian sequences was approximated by using measured thicknesses and densities of the various sublayers from different locations to give weighted averages at several distances from vent. The eruptive volumes given in Table 5a and bulk densities in the ranges 0.50–0.85 gcm^{-3} for A, 0.72–0.85 gcm^{-3} for B, 0.87–1.13 gcm^{-3} for CDE, and 0.90–1.13 gcm^{-3} for FGH were then used to calculate dense-rock equivalent (DRE) volumes in several increments at various distances from source (Appendix 1). Co-plinian distal ash volumes were incrementally converted to DRE separately from the rest of the deposits, using an estimated bulk density of 0.85–1.00 for the distal co-plinian component (Appendix 1). As magma volume is of more interest than that of fictive dense rocks, magmatic density is postulated to be 2.3 gcm^{-3} for rhyolite and 2.4 gcm^{-3} for dacite. Lithic fractions (negligible in distal ash) estimated by component analysis (Table 4) were then subtracted to yield magma volumes of 1.95 km^3 for eruptive Episode I, Phase A, 0.99 km^3 for Phase B, 1.96 km^3 for Episode II, and 1.63 km^3 for Episode III. This gives a total magma volume of ~ 6.5 km^3 emplaced as fallout, which combined with 11 ± 4 km^3 of ignimbrite (roughly 7 ± 2 km^3 DRE) yields a total magma volume of $\sim 13 \pm 3$ km^3 DRE.

Eruption durations, mass eruption rates, and column heights

The three periods of ashfall at Kodiak village are thought to correlate with the three eruptive episodes at Novarupta (Hildreth 1983), but no observers actually saw the eruption columns after the first few hours. The time from sighting of the initial column to the end of the first heavy ashfall at Kodiak was 20 h; the second ashfall reportedly lasted ~ 26 h and the third probably ~ 10 h (Griggs 1922). There need be no simple correlation, however, between downwind fallout intervals and durations of eruptive episodes at vent, owing to altitudinally variable transport velocity, wind shear, progressively slower settling of ash that systematically fines with distance, and turbulent retention of fine co-plinian ash aloft.

Some additional time constraints are provided, nonetheless, by the interfingering within the Novarupta fallout sequence of several layers of nonjuvenile lithic-rich ash expelled from Mount Katmai during collapse of its summit caldera (Hildreth 1991). The first layer of Katmai-derived lithic ash is intercalated between Novarupta-derived Layers B_2 and B_3. If this first lithic-ash layer and the first major teleseism at 2356 h (Alaskan time) on 6 June ($M_s = 6.5$; Abe 1991) both mark the onset of caldera collapse, then the first ~ 6.9 km^3 of magma (Phase A plus $\sim 2/3$ of Phase B) is constrained to have erupted within ~ 11 h. This yields an average mass eruption rate (MER) of 4.2×10^8 $kg\,s^{-1}$ for most of Episode I (including much of the main ignimbrite; Hildreth 1991).

Cessation of ashfall at Kodiak between 0900 h and 1200 h on 7 June probably means that Episode I (including the main ignimbrite phase) was over well before that. If we assume a 4-h delay between eruption and ashfall at Kodiak (based on the recorded interval of 4 h between the first sighting of the plinian column and settling of the first ash at Kodiak), Episode I lasted ~ 16 h. No similar narrative or geophysical constraints can be applied with any confidence to the durations of Episodes II or III, but their lesser complexity and smaller volumes suggest that each was shorter than Episode I. Scarcity of erosion and reworking at either the B/C contact or at the horizon of Layer E supports the inference from the fallout interruptions at Kodiak (Hildreth 1983) that breaks between eruptive episodes were no longer than a few hours.

Column height, estimated from clast-dispersal patterns, can be directly related to mass-eruption rate (MER) (Wilson et al. 1980); both have been widely used as a measure of comparison among eruptions. Using lithic clast-dispersal patterns in the fallout deposits, peak MER has been estimated for the 1912 plinian episodes following the methods of Wilson and Walker (1987), Carey and Sparks (1986), and Sparks (1986). Layers A and C yield a similar peak MER of 0.7-to-1×10^8 $kg\,s^{-1}$ for A and 0.6-to-2×10^8 $kg\,s^{-1}$ for C. Lithics in Layer F yield a lower peak MER of 2-to-4×10^7 $kg\,s^{-1}$ (Table 7). Column heights estimated from the lithic distribution following the methods of Carey and Sparks (1986) are 26 km for Phase A of Episode I, 25 km for Episode II, and 23 km for Episode III; slightly lower column heights of 23 km, 22 km, and 17–18 km are estimated following those of Wilson and Walker (1987) (Table 7).

Conclusions

Exceptional preservation of the Novarupta vent area and the compositionally zoned nature of the deposits permit uncommonly good stratigraphic correlations between proximal and distal fallout and between fallout and contemporaneous ash flows, leading to several im-

Table 7. Volcanological and modelling summary

	Episode I		Episode II	Episode III	Comments
	Plinian Phase A	Plinian Phase B	Plinian CDE	Plinian FGH	
Tephra volumes (km^3)	6.15	2.68	4.76	3.44	Fierstein and Nathenson (1992)
Magma volumes (km^3)	1.95	0.99	1.96	1.63	Rhyolite (2.3 g cm^{-3}), dacite (2.4 g cm^{-3})
Lithic volumes (km^3)	0.15	0.03	0.03	0.03	
Total DRE volumes (km^3)	2.10	1.02	1.99	1.66	Magma + lithic volumes
% Volume beyond 1-cm isopach	9	14	7	11	Fierstein and Nathenson (1992)
Radius (m) of funnel-shaped vent required to account for lithic volumes in fallout*	? (covered)	? (covered)	170 140	170 140	Assuming funnel shape yields 1 km depth Assuming funnel shape yields 1.5 km depth
Lithic lithology	Mostly Naknek; some Trident andesite; minor Falling Mtn dacite	Same as Layer A; minor vitrophyre; trace intrusives	Mostly vitrophyre; minor Naknek	Mostly vitrophyre; minor Naknek	
MER (kg s^{-1})	0.7×10^8 1×10^8	— —	0.6×10^8 $1\text{–}2\times10^8$	4×10^7 $2\text{–}3\times10^7$	Carey and Sparks (1986), Sparks (1986) Wilson and Walker (1987)
Column height (km)	26 23	— —	25 22	23 17–18	Carey and Sparks (1986) Wilson and Walker (1987)
Wind speeds (m s^{-1})	>30 15–16	— —	30 —	10 —	Carey and Sparks (1986) *Dora* ship record (Martin 1913)
Eruption duration (hrs)	11 ($A+B_1+B_2$) 16 (A thru B_3)		?	?	Using recorded teleseisms and intercalation of Katmai-derived phreatic mud layers with Novarupta plinian fallout (Hildreth 1991)
Ashfall at Kodiak (hrs)	~16 (A + B)		~26	~10	

* These are minimum vent radii because they are estimated from the volume of observed lithics in the fallout; an unknown volume of lithic lags may be buried beneath near-vent fallout

portant conclusions about the eruptive processes and dispersal of ejecta in 1912.

1. *Plinian falls and pyroclastic flows were contemporaneous.* Plinian fallout and valley-filling ignimbrite erupted contemporaneously throughout most of Episode I. This is indicated (a) by fallout layers that exhibit progressive changes in clast proportions parallel to those of the zoned ignimbrite; (b) by intercalation of Layer A with all-rhyolitic flows – including both valley-filling ignimbrite and higher-energy proximal flow veneers; and (c) by intercalation of compositionally zoned flows with comparably zoned fall Layer B. The zoned sequence of HEPIs exposed on near-vent ridges, the far more voluminous zoned sequence of valley-confined ignimbrite, and the zoned A–B plinian fallout sequence were emplaced concurrently during the same sustained plinian eruption. On a smaller scale, several intraplinian ash flows were also emplaced proximally concurrent with ejection of plinian Layers C–D and F–G during Episodes II and III. Recent experimental studies (Carey et al. 1988) suggest that volcanic plumes have a wide range of collapse behavior and that material can be simultaneously released from different levels of a sustained eruption column. The simple model of a towering plinian column abruptly terminating by collapsing to generate ash flows misrepresents the documented complexities of the 1912 eruptions (and undoubtedly of many others).

2. *Valley-filling ignimbrite with high-energy proximal facies.* Stacks of lenticular ignimbrite layers (HEPI) on ridgecrests around the Novarupta vent depression exhibit stratification resembling some surges, but their generally fines-rich nature, poor sorting, compositional zonation, stratigraphic position, and distribution show them to be elevated proximal equivalents of the main valley-filling VTTS ignimbrite. These flow veneers were deposited from the mid-to-upper zones of density-stratified ash flows and probably represent only a small fraction of the material that actually passed over the near-vent ridges. The slightly more concentrated lower zones of the same stratified flows were blocked by the ridges and directed into the main arms of the VTTS, where they deposited the volumetrically dominant, largely unstratified VFI. Flow velocities slackened so se-

Appendix 1. Converting tephra volumes to Dense Rock Equivalents (DRE)

	Fallout volume	Lithic content[a]	Bulk tephra density[b]	Fall minus lithic volume	DRE factor[c]		Magma volume	Lithic volume	Total DRE volume
Layer A									
source to 10 cm	2.64 km^3	5%	0.70 gcm^{-3} (0.50–0.85)	2.51	0.30		0.75 km^3	0.13	0.88
10 cm to 0 cm	2.46 km^3	1%	0.75 gcm^{-3} (0.72–0.79)	2.44	0.33		0.81 km^3	0.02	0.83
+ co-plinian ash (rhyolitic)	1.05 km^3	0	(0.85 gcm^{-3})	1.05	(0.37)		0.39 km^3	0.00	0.39
						TOTAL	1.95 km^3	0.15 km^3	2.10 km^3
Layer $B_1+B_2+B_3$									
source to 10 cm	0.81 km^3	2%	0.80 gcm^{-3} (0.72–0.94)	0.79	0.34		0.27 km^3	0.02	0.29
10 cm to 0 cm	1.51 km^3	1%	0.92 gcm^{-3} (0.90–0.94)	1.50	0.39		0.59 km^3	0.01	0.60
+ co-plinian ash (rhyolitic)	0.35 km^3	0	(0.85 gcm^{-3})	0.35	(0.37)		0.13 km^3	0.00	0.13
						TOTAL	0.99 km^3	0.03 km^3	1.02 km^3
Layer CDE									
source to 100 cm	1.03 km^3	2%	0.90 gcm^{-3} (0.90–0.91)	1.01	0.37		0.37 km^3	0.02	0.39
100 to 10 cm	0.68 km^3	1%	0.96 gcm^{-3} (0.87–1.05)	0.67	0.40		0.27 km^3	0.01	0.28
10 to 1 cm	0.79 km^3	0	1.02 gcm^{-3} (0.95–1.19)	0.79	0.43		0.34 km^3	0.00	0.34
1 cm to 0 cm	0.20 km^3	0	1.02 gcm^{-3} (0.96–1.13)	0.20	0.43		0.09 km^3	0.00	0.09
+ dacitic co-plinian CD ash (that settled with Layer FGH)	2.47 km^3	0	(1.00 gcm^{-3})	+2.47	(0.42)		+1.04 km^3	0.00	+1.04
-rhyolitic AB co-plinian ash (that settled with Layer CDE)	−0.41 km^3	0	(0.85 gcm^{-3})	−0.41	(0.37)		−0.15 km^3	0.00	−0.15
						TOTAL	1.96 km^3	0.03 km^3	1.99 km^3
Layer FGH									
source to 100 cm	0.60 km^3	2%	0.97 gcm^{-3} (0.90–1.03)	0.59	0.40		0.24 km^3	0.01	0.25
100 cm to 10 cm	2.46 km^3	1%	1.02 gcm^{-3} (0.94–1.09)	2.44	0.43		1.05 km^3	0.02	1.07
10 cm to 0 cm	3.99 km^3	0	1.03 gcm^{-3} (0.96–1.13)	3.99	0.43		1.71 km^3	0.00	+1.71
-rhyolitic and dacitic co-plinian ash (from AB + CDE that settled with FGH)	−3.61 km^3	0	(0.90 gcm^{-3})	−3.61	(~0.38)		−1.37 km^3	0.00	−1.37
						TOTAL	1.63 km^3	0.03 km^3	1.66 km^3
						GRAND TOTAL	6.53 km^3	0.24 km^3	6.77 km^3

[a] Approximate lithic contents in wt% are based on component analyses (see Table 4)

[b] Bulk tephra densities (ranges in parenthesis) were measured (dry) in the lab for fallout from a variety of locations relative to source; estimated values used for co-plinian ash

[c] DRE factor is the ratio between measured bulk tephra density and assumed magma density (2.3 gcm^{-3} for rhyolite, 2.4 gcm^{-3} for dacite). Estimated DRE factors (in parenthesis) are used where there is no measured bulk tephra density

verely down-valley that in the lower VTTS the main ash flows were unable to override even minor topographic obstacles.

3. *Plinian fallout with sectorially contrasting characteristics.* Few plinian deposits exhibit radially symmetrical thickness distribution (circular concentric isopachs), but in addition to a variety of isopach patterns (Figs. 5 and 14) the 1912 plinian deposits show marked sectorial contrasts in grainsize, composition and internal subdivisions. Although Episode II fallout 10–15 km downwind consists of one thick, poorly graded deposit (C) and one thin, normally graded deposit (D), it forms a sequence of three normally graded layers (C_1, C_2, and D) 10 km NW of vent. Episode III fallout is subdivided into two poorly graded deposits (F and G) NE of Novarupta, but equivalent deposits S and SE of vent consist of three distinctly graded fall layers (F_1, F_2, and G). Sectorial distinctions in the number and character of internal subunits may reflect asymmetrical expansion of the umbrella region of the eruption cloud and altitudinally variable wind directions and turbulence, and not necessarily any significant syneruptive change in vent configuration, MER, or column height. For the 1912 plinian layers, deposits along downwind dispersal axes do not adequately represent the range of variability in subunit stratification, grainsize, componentry, or rate of change of thickness with distance observed along off-axis azimuths.

4. *Fine ash suspended in the atmosphere settled with that from subsequent eruptive episodes. Widely dispersed fine ash can be co-plinian rather than co-ignimbrite.* The uppermost fall layer that accumulated toward the SE during and after dacitic Episode III contains a large fraction of rhyolite (up to 40% on Kodiak Island) not present in equivalent proximal deposits (99% dacitic and 1% rhyolitic pumice near Novarupta). The uppermost ash layer is thus strongly *composite,* consisting of shards from earlier rhyolitic and subsequent dacitic eruptive episodes. Microprobe analyses of downwind ash show that similar mixing relations also variably characterize Layers B through G, each successive eruptive pulse incorporating some of the fine ash held aloft between eruptions. Only a small fraction of the rhyolite in the distal layers of Episodes II and III was recycled from near-vent deposits because (1) excluding the base of C, the thick proximal blanket of dacite pumice-fall deposits contains few rhyolitic clasts; (2) the vent was smaller during the dacitic episodes than during Episode I; and (3) Episode I material backfilling the vent was by then largely welded. In locations close to the rhyolite-dominated VTTS ignimbrite, fine-grained Layers E and H are largely dacitic, so they do not contain a major contribution of co-ignimbrite ash. In the distal downwind sector, the abundant rhyolitic shards in the upper layers on both sides of Shelikof Strait represent fine ash that lingered aloft, left over from the plinian eruptions of Phases A and B and, accordingly, are here referred to as a 'co-plinian' ash contribution. Layers CDE and FGH together contain as much as 1.5 km^3 of this distal Episode I rhyolitic ash. Breaks-in-slope for 1912 plinian data on plots of log thickness versus area$^{1/2}$ largely reflect decoupling in the settling behavior of plinian and co-plinian ash, respectively coarser and finer than ~250 μm.

Acknowledgements. This manuscript has been helped along the way by especially fruitful discussions with Tim Druitt, Bruce Houghton, Gail Mahood, and Colin Wilson. Rainy field seasons in Alaska were made brighter by Mahood, Rick Hutchinson, Terry Keith, Tina Neal, and Jim Riehle. Captain Eric Stirrup of Kodiak Sea Charters and first mate, Hank Pennington, always found safe harbors during our tephra search along the Shelikof Strait coastlines. Perry Mollan skippered a Naknek Lake tephra reconnaissance. Riehle and Maura Hanning measured several sections. The National Park Service staff made our visits to Brooks Camp comfortable, and Eric Schmidt contributed much-appreciated leftover sandwiches to our spartan menu. Manny Nathenson added mathematical expertise and Peggy Bruggman and Ellen Lougee provided technical assistance. Helpful reviews by Houghton, Riehle, Wilson, Armin Freundt, and Jocelyn McPhie are greatly appreciated. Suggestions and comments by Paul van den Bogaard, Bob Christiansen, Mauro Rosi, Hans-Ulrich Schmincke, Steve Self, and Mari Sumita were stimulating and helpful. Many thanks to all.

References

Abe K (1992) Seismicity of the great eruption of Mount Katmai, Alaska, in 1912. Bull Seism Soc Am 82:175–191

Carey SN, Sigurdsson H (1982) Influence of particle aggregation on deposition of distal tephra from the May 18, 1980, eruption of Mount St. Helens volcano. J Geophys Res 87:7061–7072

Carey S, Sparks RSJ (1986) Quantitative models of the fallout and dispersal of tephra from volcanic eruption columns. Bull Volcanol 48:109–125

Carey SN, Sigurdsson H, Sparks RSJ (1988) Experimental studies of particle-laden plumes. J Geophys Res 93:15314–15328

Curtis GH (1968) The stratigraphy of the ejecta from the 1912 eruption of Mount Katmai and Novarupta, Alaska. Geol Soc Am Mem 116:153–210

Federman AN, Scheidegger KF (1984) Compositional heterogeneity of distal tephra deposits from the 1912 eruption of Novarupta, Alaska. J Volcanol Geotherm Res 21:233–254

Fierstein J, Nathenson M (1992) Another look at the calculation of fallout tephra volumes. Bull Volcanol 54:156–167

Fisher RV, Schmincke H-U (1984) Pyroclastic rocks. Springer-Verlag, Berlin, Heidelberg, New York, Tokyo, 472 pp

Freundt A, Schmincke H-U (1986) Emplacement of small-volume pyroclastic flows at Laacher See (East-Eifel, Germany). Bull Volcanol 48:39–59

Froggatt PC (1982) Review of methods of estimating rhyolitic tephra volumes; applications to the Taupo Volcanic Zone, New Zealand. J Volcanol Geotherm Res 14:301–318

Griggs RF (1922) The Valley of Ten Thousand Smokes. National Geogr Soc, Washington, 340 pp

Hildreth W (1983) The compositionally zoned eruption of 1912 in the Valley of Ten Thousand Smokes, Katmai National Park, Alaska. J Volcanol Geotherm Res 18:1–56

Hildreth W (1987) New perspectives on the eruption of 1912 in the Valley of Ten Thousand Smokes, Katmai National Park, Alaska. Bull Volcanol 49:680–693

Hildreth W (1991) The timing of caldera collapse at Mount Katmai in response to magma withdrawal toward Novarupta. Geophys Res Lett 18:1541–1544

Hildreth W, Drake R (1992) Volcán Quizapu, Chilean Andes. Bull Volcanol 54:93–125

Imman DL (1952) Measures for describing the size distribution of sediments. J Sediment Petrol 22:125–145

Martin GC (1913) The recent eruption of Katmai volcano in Alaska. National Geog Mag 24:131–181

Nayudu YR (1964) Volcanic ash deposits in the Gulf of Alaska and problems of correlation of deep-sea ash deposits. Marine Geol 1:194–212

Pyle DM (1989) The thickness, volume and grainsize of tephra fall deposits. Bull Volcanol 51:1–15

Pyle DM (1990) New estimates for the volume of the Minoan eruption. In: Hardy D (ed) Thera and the Aegean World III, 2, Earth Sciences, The Thera Foundation London, pp 113–121

Rose WI Jr, Bonis S, Stoiber RE, Keller M, Bickford T (1973) Studies of volcanic ash from two recent Central American eruptions. Bull Volcanol 37:338–364

Rosi M (1992) A model for the formation of vesiculated tuff by the coalescence of accretionary lapilli. Bull Volcanol 54:429–434

Schumacher R (1990) Artificial ash clusters and deposition of fine volcanic ash (abstract). IAVCEI, International Volcanol Congress, Mainz (FRG), Abstracts volume, unpaginated

Schumacher R, Schmincke H-U (1990) The lateral facies of ignimbrites at Laacher See volcano. Bull Volcanol 52:271–285

Sigurdsson H, Carey SN, Cornell W, Pescatore T (1985) The eruption of Vesuvius in AD 79. Nat Geog Res 1:332–387

Sparks RSJ (1976) Grain size variations in ignimbrites and implications for the transport of pyroclastic flows. Sedimentology 23:147–188

Sparks RSJ (1986) The dimensions and dynamics of volcanic eruption columns. Bull Volcanol 48:3–15

Sparks RSJ, Walker GPL (1977) The significance of vitric-enriched air-fall ashes associated with crystal-enriched ignimbrites. J Volcanol Geotherm Res 2:329–341

Thorarinsson S (1954) The tephra fall from Hekla on March 29th, 1947. In: The eruption of Hekla 1947–1948, II. Soc Scient Islandica 1:1–68

Valentine G (1987) Stratified flow in pyroclastic surges. Bull Volcanol 49:616–630

Walker GPL (1971) Grain-size characteristics of pyroclastic deposits. J Geol 79:696–714

Walker GPL (1980) The Taupo pumice: product of the most powerful known (ultraplinian) eruption? J Volcanol Geotherm Res 8:69–94

Walker GPL (1981) Plinian eruptions and their products. Bull Volcanol 44:223–240

Walker GPL, Croasdale R (1971) Two plinian-type eruptions in the Azores. J Geol Soc London 127:17–55

Walker GPL, Wilson L, Bowell ELG (1971) Explosive volcanic eruptions – I. The rate of fall of pyroclasts. Geophys J R Astron Soc 22:377–383

Walker GPL, Wilson CJN, Froggatt PC (1981) An ignimbrite veneer deposit: the trail-marker of a pyroclastic flow. J Volcanol Geotherm Res 9:409–421

Wallmann PC, Pollard DD, Hildreth W, Eichelberger JC (1990) New structural constraints on magma chamber locations at the Valley of Ten Thousand Smokes, Katmai National Park, Alaska. Geology 18:1240–1243

Wilson L (1972) Explosive volcanic eruptions – II. The atmospheric trajectories of pyroclasts. Geophys J R Astron Soc 30:381–392

Wilson L, Huang TC (1979) The influence of shape on the atmospheric settling velocity of volcanic ash particles. Earth Planet Sci Lett 44:311–324

Wilson L, Walker GPL (1987) Explosive volcanic eruptions – VI. Ejecta dispersal in plinian eruptions: the control of eruption conditions and atmospheric properties. Geophys J R Astron Soc 89:657–679

Wilson L, Sparks RSJ, Walker GPL (1980) Explosive volcanic eruptions – IV. The control of magma properties and conduit geometry on eruption column behavior. Geophys J R Astron Soc 63:117–148

Editorial responsibility: B. F. Houghton